

Received: 28.09.2024

Accepted: 20.11.2024

Research Article

An in silico investigation of pyrazole, indazole, and imidazopyridine analogs as inhibitors for SRC tyrosine kinase, key enzyme regulating malignancies in various tumors

Rashmi P^{a,1}, Vishak Harish^b

^aProfessor and Head, Department of Pharmaceutical Chemistry, Mallige College of Pharmacy, #71, Silvepura Road, Chikkabanavara Post, Bengaluru 560090, Karnataka, India.

^bStudent, BSc, Nrupathunga University, Nrupathunga Road, Bengaluru 560001, Karnataka, India.

Abstract: Tyrosine kinases are considered as major target in the treatment of cancer as they regulate various cellular metabolic pathways. SRC tyrosine kinase is one of the key enzyme involved in various cellular processes and is considered a promising therapeutic target for cancer treatment. In silico computational studies were carried out to evaluate the potential of pyrazole, indazole, and imidazopyridine analogs as SRC (commonly known for c-SRC, pronounced as a short form of sarcoma) kinase inhibitors. Molegro Virtual Docker version 2019.7.0.0-2019-03-18 was used to screen a large number of pyrazole, indazole, and imidazopyridine analogs. The top ligands were selected based on their binding affinity and further analyzed for their interactions with the SRC kinase binding site. The results showed that many of the analogs interacted with key amino acid residues of the DFG motif, Asp-404, Phe-405, and Gly-406, and the hinge region, Glu-339, Tyr-340, and Met-341 including gatekeeper residue Thr-338 of the enzyme. In silico ADMET studies were performed to assess the pharmacokinetic and toxicological properties of the selected ligands. The results indicated that most of the ligands had good oral absorption and favorable protein binding. However, some ligands showed potential toxicity, including hepatotoxicity and drug-induced liver injury. MD Simulations were conducted to study the stability and interactions between the ligands and SRC kinase over a 25 ns period. The simulations revealed that most of the complexes remained stable, and the best ones are 71588244 and 70736676. The findings suggest that these analogs could be further developed as potential therapeutic agents for the treatment of cancer.

Keywords: SRC Kinase, Docking based virtual screening, In silico studies, Pyrazole, MD simulations, Indazole

1. Introduction

Tyrosine kinases are a group of enzymes that catalyze the phosphorylation of tyrosine residue in various protein substrates. These enzymes regulate the processes of metabolism, apoptosis, cell division, and growth using Adenosine Tri Phosphate (ATP). The two main categories of tyrosine kinases based on location are non-receptor tyrosine kinases (NRTK) and receptor tyrosine kinases (RTK). SRC (commonly known for c-SRC, pronounced as a short form of sarcoma) and ABL (abelson) tyrosine kinases are examples of NRTKs, whereas EGFR (Endothelial Growth Factor

Receptor), and VEGFR (Vascular Endothelial Growth Factor Receptor) tyrosine kinases are examples of RTKs [1].

The major function of tyrosine kinases is to phosphorylate particular amino acids on enzymes, that subsequently alter signal transduction. Owing to their crucial function in signal transduction, they have emerged as the main targets of cancer-targeted treatment. A new class of drugs called tyrosine kinase inhibitors (TKIs) has been developed and more than 50 tyrosine kinase inhibitors were approved for the treatment of various types of cancers in the last twenty years [2,3]. Among

¹ Corresponding Authors

e-mail: dr.rashmip123@gmail.com

various tyrosine kinase families, SRC is a family of 11 members belonging to NRTKs which are collectively called SRC Family Kinases (SFK). As this family is involved in the regulation of cell cycle progression, differentiation, motility, proliferation, and survival to sustain homeostasis, their overexpression and deregulation are observed in various malignancies [4]. Numerous malignancies, including pancreatic, prostate, lung, breast, and a few other epithelial and non-epithelial tumors, have been shown to have abnormally activated and/or overexpressed SFKs. Since SFKs control several signaling pathways related to angiogenesis, metastasis, proliferation, and survival, they are considered to be useful therapeutic targets for preventing tumors from spreading to a metastatic stage [5, 6].

SRC, a protooncogene, has been extensively studied due to its role in cellular metabolism and growth as well as being a node of communication for many proteins in different signaling pathways [7]. SRC regulates receptor signaling, which impacts various cellular processes associated with cell transformation such as metabolism, proliferation, apoptosis, and cell adhesion. So, SRC kinase activity is considered significant in several aspects like tumor progression, including proliferation, migration, invasion, angiogenesis, chemoresistance, stemness, and metastasis [8]. SRC activation promotes the dissociation of cell-cell adhesion junctions by interacting with p120 catenin and facilitates cell mobility. SRC activation induces the formation of invadopodia and invadopodia-mediated matrix degradation. It also enhances the stability of focal adhesion complexes consisting of FAKs, i.e., focal adhesion kinase. SRC kinase also plays a role in the viability of disseminated cells and metastatic recurrence once the cells reach distant organs. Another important role after SRC activation is to regulate the formation of actin stress fibers that are necessary for the outgrowth of metastatic cells. Saracatinib is successful in suppressing this outgrowth. The SRC activation makes the tumor cells resistant to anoikis [9]. Consequently, inhibiting SRC kinase has become a promising approach, and in recent years, many small molecules inhibiting SRC kinase have been developed to treat various cancers like colorectal cancer [10] and breast cancer [11], etc. There are many inhibitors reported targeting SRC

[12, 13] and approved (ibrutinib, bosutinib) for the treatment of cancer [14, 15]. SRC inhibitors, despite being used as successful therapeutic agents in cancer, and proved to reduce the risk of relapse, progression, and death in cancer patients, few of them developed resistance to these drugs even after initial progress. Mutations in the BCR (Breakpoint cluster)-ABL kinase ATP binding and catalytic domain were reported to be the reason for the development of resistance [16]. Profiling of SRC tyrosine kinase mutants was carried out to analyze and find the residues that undergo mutation leading to resistance to inhibitors by lowering the affinity and promoting hyperactivation [17]. Accordingly, there is a need and much scope is there for the discovery of new SRC tyrosine kinase inhibitors. In this view, our current research work attempts to explore the possibility of discovering the new lead molecules among, pyrazoles, indazoles, and imidazopyridine analogs for SRC kinase inhibition by employing docking-based virtual screening (DBVS) followed by molecular docking, in silico ADMET (absorption, distribution, metabolism, excretion, toxicity) studies, and Molecular Dynamics simulations.

2. Computational Method

2.1. Virtual Screening and Molecular Docking Studies

Virtual screening and all molecular docking simulations were carried out using Molegro Virtual Docker (MVD) [18] version 2019.7.0.0-2019-03-18. The crystal structure of C-SRC in complex with Ibrutinib [PDB: 6L8L] (2.89 Å resolution) was downloaded from the RCSB Protein Data Bank. Using Discovery Studio Visualiser [19], the water molecules and ligands were removed from the protein, and Chain A was taken for further studies. The protein (Chain A) was imported into MVD, and the hybridization states, missing bond orders, and angles were then assigned. To find potential binding sites cavities were detected in the protein, and a maximum of five cavities were found. In cavity number 1, (Volume-451.72), space occupied by ibrutinib was chosen for further studies with a grid resolution of 0.30 Å and 10 Å radius. The search algorithm was set to GPU Screening (CUDA) and the scoring function was Plants [GRID] in virtual screening mode with a 5% return of best poses. All ligand structures were

Rashmi P, Vishak Harish

downloaded in 3D sdf format with 1 conformer from the PubChem database [PubChem: Pyrazoles, Imidazopyridines, Indazoles] after applying filters according to Lipinski's Rule of 5.

Validation of the docking protocol was done by re-docking the co-crystallized ibrutinib with the

protein 6L8L and comparing the bound ibrutinib with docked ibrutinib. Docking results show that the resulted pose was in the same space and same orientation indicating that the protocol is acceptable which is shown in Fig 1.

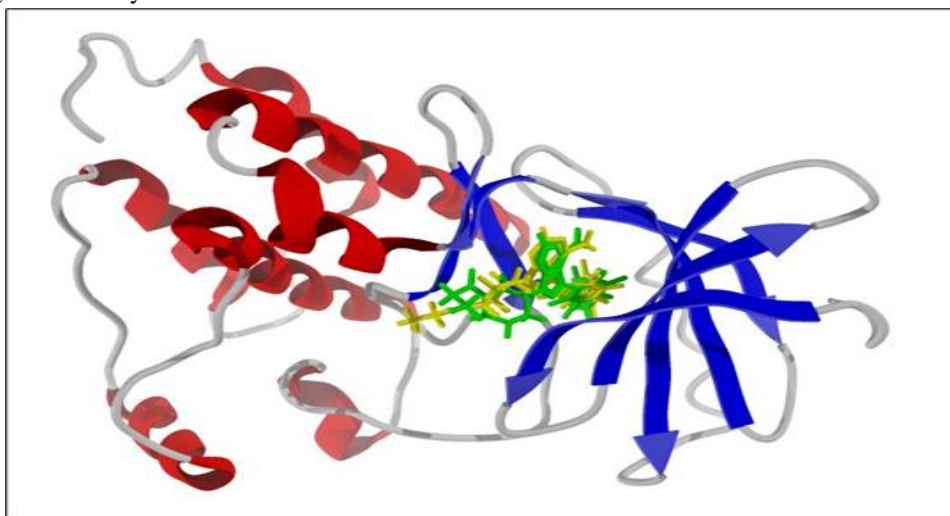


Figure 1. Overlapping of docked ibrutinib with bound ibrutinib in the binding pocket of 6L8L. Yellow-docked ibrutinib, green-bound ibrutinib

These ligands were imported to MVD and prepared while importing. The search space was confined to the space occupied by Ibrutinib and virtual screening was done using the GPU scoring search algorithm and MolDock [GRID] scoring function. The top 5% of returned poses were exported as ligands and further subjected to detailed docking studies with default settings using the MolDock SE search algorithm and MolDock [GRID] scoring function. (Plant score [GRID] was not considered because during trials, positive controls chosen as reference points were shown random results). The identification of ligand binding modes was done by iteratively evaluating several candidate solutions (ligand conformations) and estimating the energy of their interactions with the macromolecule. Docking was done in multiple processes using the CPU (Central Processing Unit). Docking results were analyzed using the pose organizer, and ligand map.

2.2. In silico ADMET prediction

Pharmacokinetic properties like ADME along with toxicities of selected ligand molecules were predicted using the web server ADMETlab 2.0 [20]. Physicochemical properties like log S, log P, and log D values and toxicological properties like carcinogenicity, respiratory toxicity, skin

sensitivity, etc were also predicted using the same server. SMILES of all ligands were uploaded to the server and screened for ADMET. The data generated was exported to Excel file format for further analysis. In addition to these, drug likeliness and synthetic accessibility have also been analyzed.

2.3. MD simulations

The MD simulations were done using GROMACS software [21-24] in a Linux environment. The selected ligands were exported as mol2 files. The ligands were then processed in Chimera as hydrogens were to be added to the existing ligand files to facilitate proper MD simulations. Chimera is free software that was used to edit the ligand structures as required [25]. After confirming the error-free structures of the ligands, a Perl script was executed to arrange the bonds of the ligands in ascending order, as various software create bond orders in different sequences. Otherwise, it will be difficult to create topology files for the ligands which are required for MD.

After the topology was generated for the ligand molecule the topology files, ligand file, and protein file were saved separately. Then the protein file was prepared using GROMACS, where structural errors were rectified, if any. The CHARMM27 force field

[26-28] (chemistry at Harvard macromolecular mechanics) was used, which is an all-atom force field, and the TIP3P (transferable intermolecular potential 3P) water model was used for the same. CHARMM27 force field has been widely tested and validated by many researchers. It has been proven efficient and error-free for the simulation calculation. CHARMM27 is an updated version of CHARMM22. While CHARMM22 is exclusively for only for protein systems, whereas CHARMM27 has been enhanced for DNA simulations as well. The CHARMM27 or the CHARMM22 force field has been selected because it takes into consideration the Urey-Bradley term. The Urey-Bradley term is responsible for keeping the system from simulating unconventional bond angles between three bonded atoms. This component sets a fixed value for the energy and angle for the bonded atoms, this energy is known as the equilibrium value or the relaxed state for the atoms. During the simulation, if the bond angle of these three atoms changes greater than a certain limit, then this term compensates energy in accordance of the change to the system to compensate for the change in the bond angle of the atoms. This can be addition of energy to the total energy of the system. If this additional energy is not added to the system the structure of the molecule can become highly strained, leading to unwanted structural configurations. This can impact the final result in a negative way. In order to avoid improbable bond angles in the simulation the Urey-Bradley term is very important in predicting accurate structures and the change in structures during the MD process. The TIP3P water model was used because of its lower computational cost while offering good accuracy. In the TIP3P model, the water is modelled with the help of Lennard-Jones potentials to take van der Waal interactions between the water molecules into consideration, and Coulomb's Law to include the electrostatic interactions between the charged ions. We say less computational cost because in this model the water molecule is assumed to be rigid i.e., the bond length and the bond angle of the water molecule are taken to be constant and do not vary over time. The topology files for the protein were generated using in-built commands in GROMACS. The data from the topology files of the ligand were copied to the topology file of the protein for further processing.

The Energy minimization was done using the "Steepest Energy Minimization" algorithm, where the minimization was stopped when the maximum force < 10.0 kJ/mol with 0.01 being the energy step size. Further, equilibration simulations were run viz., NVT and NPT equilibration. NVT equilibration is done to bring the system to the desired temperature i.e., 300K in our case. This equilibration stabilizes the system at the given temperature. Whereas the NPT equilibration is done to stabilize the system to the set pressure (101325 Pa). Both the simulations were done for 2 ns each using GROMACS.

The protein was put in a triclinic box and solvated [29] with water. The overall charge of the proteins was balanced with Sodium and Chloride ions. Lastly, the Molecular Dynamics calculations were done for the protein-ligand complex. The simulation was run for 25 ns for each ligand. The change in energies of the system was saved every 10 ps. The step change was 2 fs. After the MD was done, the protein was centered in the generated box. RMSD was calculated for the ligand, and RMSF was calculated for the protein chain. Next, the hydrogen bonds between the protein and ligand were analyzed and graphed. Also, the gyration radius was calculated for the protein chain. At last, the total energy and the temperature of the protein-ligand complex were calculated.

3. Results and discussion

3.1. Virtual screening and molecular docking studies

Virtual screening based on molecular docking has gained popularity in recent years, providing an additional means of high throughput screening during the hit identification and lead optimization phases [30]. In our current research, we employed DBVS to identify the hits for the inhibition of SRC kinase. SRC kinase complexed with Ibrutinib (PDB id: 6L8L) was considered for the current study, where the DFG motif is in an intermediate conformation. (DFG partially out) [31]. Small molecules having pyrazole, indazole, and imidazopyridine cores, that are considered probable hinge binders [32, 33] were analyzed for their interaction with SRC kinase.

Around 9,40,000 pyrazole analogs were filtered according to Lipinski's rule to get 112335 molecules from PubChem. Similarly, 104270

Rashmi P, Vishak Harish

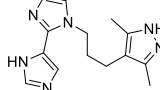
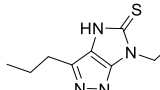
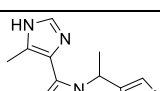
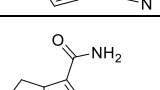
molecules were filtered to get 13136 molecules of imidazopyridine analogs, and 624703 molecules were filtered to get 20844 molecules of indazole analogs. Virtual screening was done separately for pyrazole analogs. Imidazopyridine analogs and indazole analogs were screened together due to the smaller number of analogs compared to pyrazole analogs. The search space was limited to the space occupied by Ibrutinib. The molecules were ranked based on the Moldock score, and the top five percent of returned ligands, 5615 were taken for further docking studies. Along with them Ibrutinib, Bosutinib, Dasatinib, Elzovantinib, Ruxolitinib, and Saracatinib, which are known SRC kinase inhibitors, were taken as positive controls, and Ibuprofen, Mefenamic acid, Paracetamol, and Piroxicam that are non-inhibitors of SRC kinase were taken as negative controls for the docking process as checkpoints. Docking results are given in Table 1.

The binding affinity given under the MolDock score was considered for assessment because it matches the trend of positive and negative controls. The ligands whose binding affinity was near or greater than the positive control with the least binding affinity (Elzovantinib) were considered for further analysis as it was the least binding affinity among the positive controls. Negative controls' best binding affinity was -104.73. Hence, ligands with MolDock scores less than or equal to -126 were considered to have good results. A total of 278 ligands from the pyrazole class of analogs and 708 ligands belonging to the indazole and imidazopyridine class of analogs were considered; results are available in supporting information. Among these, the top twenty-five ligands from each class were considered for analysis of interactions at the binding site, and the docking results are given in Tables 2 and 3, respectively. Docking results of best poses are shared in the supplementary material.

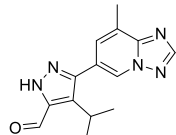
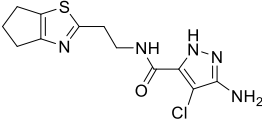
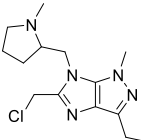
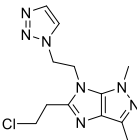
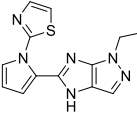
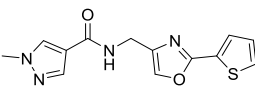
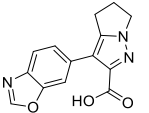
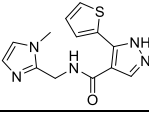
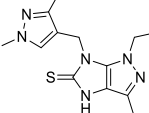
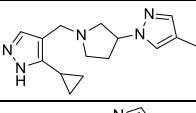
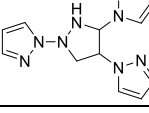
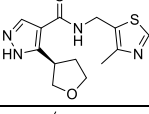
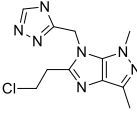
Table 1. Docking results of positive and negative controls

Sl. No.	Ligand	MolDock Score	Rerank Score	HBond
1	Ibrutinib (+)	-162.84	-132.668	-4.91474
2	Bosutinib (+)	-154.368	-122.235	-0.547035
3	Saracatinib (+)	-142.178	-110.791	-5.40621
4	Ruxolitinib (+)	-138.571	-81.3391	-3.66167
5	Dasatinib (+)	-130.979	-109.392	-3.8659
6	Elzovantinib (+)	-126.113	-105.322	-4.9855
7	Piroxicam (-)	-104.73	-44.3681	-5.89052
8	Mefenamic acid (-)	-93.573	-79.9718	-4.42001
9	Ibuprofen (-)	-85.9425	-74.7829	-4.99087
10	Paracetamol (-)	-68.5994	-59.2712	-4.99061

Table 2. Docking results of pyrazole analogs

Sl. No.	PubChem Id	IUPAC Name	Structure	Moldock Score	H-Bond
1	70736676	4-[3-[2-(1H-imidazol-5-yl)imidazol-1-yl]propyl]-3,5-dimethyl-1H-pyrazole		-143.25	-2.26713
2	106405701	1-methyl-6-[2-(1,2,4-oxadiazol-3-yl)ethyl]-3-propyl-4H-imidazo[4,5-c]pyrazole-5-thione		-138.967	-5.92872
3	56861793	1-methyl-4-[1-[2-(5-methyl-1H-imidazol-4-yl)imidazol-1-yl]ethyl]pyrazole		-138.312	-7.59102
4	4768943	N-(3-carbamoyl-5,6-dihydro-4H-cyclopenta[b]thiophen-2-yl)-1-methylpyrazole-3-carboxamide		-137.96	-2.10139

Rashmi P, Vishak Harish

Table 2. Docking results of pyrazole analogs					
Sl. No.	PubChem Id	IUPAC Name	Structure	Moldock Score	H-Bond
5	156321592	3-(8-methyl-[1,2,4]triazolo[1,5-a]pyridin-6-yl)-4-propan-2-yl-1H-pyrazole-5-carbaldehyde		-137.833	-5.81515
6	91772399	3-amino-4-chloro-N-[2-(5,6-dihydro-4H-cyclopenta[d][1,3]thiazol-2-yl)ethyl]-1H-pyrazole-5-carboxamide		-137.478	-9.7214
7	106020530	5-(chloromethyl)-3-ethyl-1-methyl-6-[(1-methylpyrrolidin-2-yl)methyl]imidazo[4,5-c]pyrazole		-137.012	-1.26869
8	104447491	5-(2-chloroethyl)-1,3-dimethyl-6-[2-(triazol-1-yl)ethyl]imidazo[4,5-c]pyrazole		-136.798	-6.18519
9	135966420	2-[2-(1-ethyl-4H-imidazo[4,5-c]pyrazol-5-yl)pyrrol-1-yl]-1,3-thiazole		-136.503	-2.70789
10	41709670	1-methyl-N-[(2-thiophen-2-yl-1,3-oxazol-4-yl)methyl]pyrazole-4-carboxamide		-136.109	-4.55005
11	84206551	3-(1,3-benzoxazol-6-yl)-5,6-dihydro-4H-pyrrolo[1,2-b]pyrazole-2-carboxylic acid		-136.075	-5.82886
12	119066539	N-[(1-methylimidazol-2-yl)methyl]-5-thiophen-2-yl-1H-pyrazole-4-carboxamide		-135.989	-2.61878
13	115990819	6-[(1,3-dimethylpyrazol-4-yl)methyl]-1-ethyl-3-methyl-4H-imidazo[4,5-c]pyrazole-5-thione		-135.73	-2.53946
14	126947450	1-[1-[(5-cyclopropyl-1H-pyrazol-4-yl)methyl]pyrrolidin-3-yl]-4-methylpyrazole		-135.707	-2.93942
15	90935652	1-[1,3-di(pyrazol-1-yl)pyrazolidin-4-yl]pyrazole		-135.54	-3.71603
16	129327913	N-[(4-methyl-1,3-thiazol-5-yl)methyl]-5-[(3R)-oxolan-3-yl]-1H-pyrazole-4-carboxamide		-135.538	-4.74765
17	79288542	5-(2-chloroethyl)-1,3-dimethyl-6-[(4-methyl-1,2,4-triazol-3-yl)methyl]imidazo[4,5-c]pyrazole		-135.399	-1.58315

Rashmi P, Vishak Harish

Table 2. Docking results of pyrazole analogs

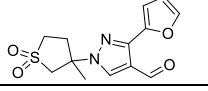
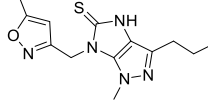
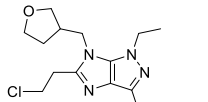
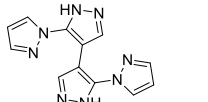
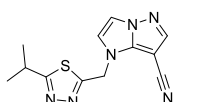
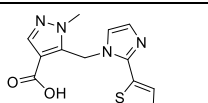
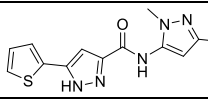
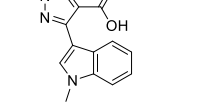
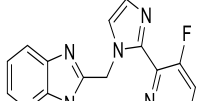
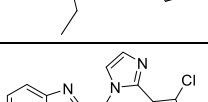
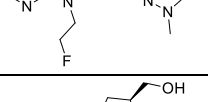
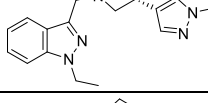
Sl. No.	PubChem Id	IUPAC Name	Structure	Moldock Score	H-Bond
18	60924396	3-(furan-2-yl)-1-(3-methyl-1,1-dioxothiolan-3-yl)pyrazole-4-carbaldehyde		-135.394	-2.43263
19	79300032	1-methyl-6-[(5-methyl-1,2-oxazol-3-yl)methyl]-3-propyl-4H-imidazo[4,5-c]pyrazole-5-thione		-135.241	-3.94882
20	79307329	5-(2-chloroethyl)-1-ethyl-3-methyl-6-(oxolan-3-ylmethyl)imidazo[4,5-c]pyrazole		-135.232	-2.80051
21	57122893	5-pyrazol-1-yl-4-(5-pyrazol-1-yl-1H-pyrazol-4-yl)-1H-pyrazole		-135.217	-6.93168
22	132318830	1-[(5-propan-2-yl-1,3,4-thiadiazol-2-yl)methyl]imidazo[1,2-b]pyrazole-7-carbonitrile		-135.175	-5.5413
23	116630266	1-methyl-5-[(2-thiophen-2-yl)imidazol-1-yl)methyl]pyrazole-4-carboxylic acid		-135.074	-4.35413
24	60509598	N-(2,5-dimethylpyrazol-3-yl)-5-thiophen-2-yl-1H-pyrazole-3-carboxamide		-134.994	-5.14737
25	116864159	1-ethyl-3-(1-methylindol-3-yl)pyrazole-4-carboxylic acid		-134.967	-3.02409

Table 3. Docking results of indazole and imidazopyridine analogs

Sl. No.	Pub chem Id	IUPAC Name	Structure	Moldock Score	H-Bond
1	22380154	3-Ethyl-2-[[2-(3-fluoropyridin-2-yl)imidazol-1-yl)methyl]imidazo[4,5-b]pyridine		-159.596	-2.26713
2	22380093	2-[[2-(4-chloro-1-methylpyrazol-3-yl)imidazol-1-yl)methyl]-3-(2-fluoroethyl)imidazo[4,5-b]pyridine		-155.427	-5.92872
3	120602685	1-[(1-ethylindazol-3-yl)methyl]-4-(1-methylpyrazol-4-yl)pyrrolidin-3-yl]methanol		-154.241	-7.59102
4	142663274	2-[[2-(2,5-dimethyl-1,3-dihydropyrazol-3-yl)imidazol-1-yl)methyl]-3-propylimidazo[4,5-b]pyridine		-153.102	-2.10139

Rashmi P, Vishak Harish

Table 3. Docking results of indazole and imidazopyridine analogs

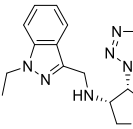
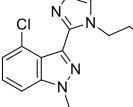
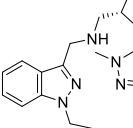
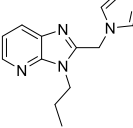
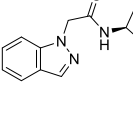
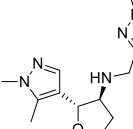
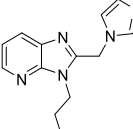
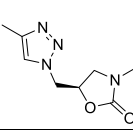
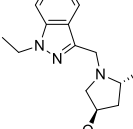
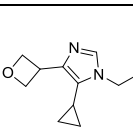
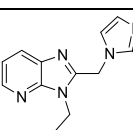
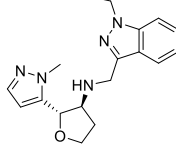
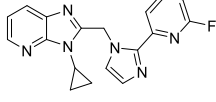
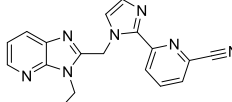
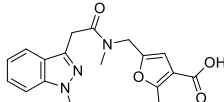
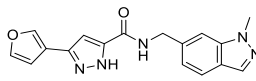
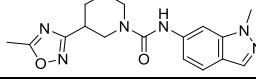
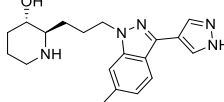
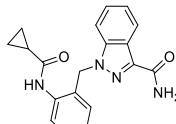
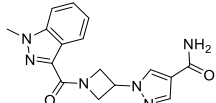
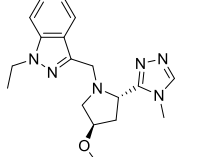
Sl. No.	Pub chem Id	IUPAC Name	Structure	Moldock Score	H-Bond
5	137968568	(3R,4S)-N-[(1-ethylindazol-3-yl)methyl]-4-(triazol-1-yl)oxolan-3-amine		-152.934	-5.81515
6	136102669	3-[2-[2-(4-chloro-1-methylindazol-3-yl)imidazol-1-yl]ethyl]-1,4-dihydro-1,2,4-triazol-5-one		-152.21	-9.7214
7	120431098	N-[(1-ethylindazol-3-yl)methyl]-1-[(2R,3S)-2-(2-methylpyrazol-3-yl)oxolan-3-yl]methanamine		-151.932	-1.26869
8	22380098	2-[[2-(4-chloro-1-methylpyrazol-3-yl)imidazol-1-yl]methyl]-3-propylimidazo[4,5-b]pyridine		-151.393	-6.18519
9	72859965	2-indazol-1-yl-N-[(3R,4S)-4-[(3-methyl-1,2-oxazol-5-yl)methyl]oxolan-3-yl]acetamide		-150.785	-2.70789
10	137865110	(2R,3S)-2-(1,5-dimethylpyrazol-4-yl)-N-[(1-ethylindazol-3-yl)methyl]oxolan-3-amine		-150.441	-4.55005
11	22380297	2-[[2-(1,5-dimethylpyrazol-3-yl)imidazol-1-yl]methyl]-3-propylimidazo[4,5-b]pyridine		-149.127	-5.82886
12	24738083	(5R)-5-[(4-methyltriazol-1-yl)methyl]-3-(1-propan-2-ylindazol-5-yl)-1,3-oxazolidin-2-one		-148.242	-2.61878
13	128979665	1-ethyl-3-[[[(2S,4R)-4-methoxy-2-(5-methyl-1H-1,2,4-triazol-3-yl)pyrrolidin-1-yl]methyl]indazole		-147.463	-2.53946
14	166048341	3-cyclopropyl-5-[[5-cyclopropyl-4-(oxetan-3-yl)imidazol-1-yl]methyl]imidazo[4,5-b]pyridine		-147.045	-2.93942
15	20812083	2-[[2-(1-methylpyrazol-3-yl)imidazol-1-yl]methyl]-3-propylimidazo[4,5-b]pyridine		-146.93	-3.71603

Table 3. Docking results of indazole and imidazopyridine analogs

Sl. No.	Pub chem Id	IUPAC Name	Structure	Moldock Score	H-Bond
16	128976367	(2S,3S)-N-[(1-ethylindazol-3-yl)methyl]-2-(2-methylpyrazol-3-yl)oxolan-3-amine		-146.583	-4.74765
17	20812061	3-cyclopropyl-2-[[2-(6-fluoropyridin-2-yl)imidazol-1-yl]methyl]imidazo[4,5-b]pyridine		-146.207	-1.58315
18	20812045	6-[1-[(3-ethylimidazo[4,5-b]pyridin-2-yl)methyl]imidazol-2-yl]pyridine-2-carbonitrile		-146.089	-2.43263
19	122107656	2-methyl-5-[[methyl-[2-(1-methylindazol-3-yl)acetyl]amino]methyl]furan-3-carboxylic acid		-145.825	-3.94882
20	146126560	3-(furan-3-yl)-N-[(1-methylindazol-6-yl)methyl]-1H-pyrazole-5-carboxamide		-145.799	-2.80051
21	72865216	N-(1-methylindazol-6-yl)-3-(5-methyl-1,2,4-oxadiazol-3-yl)piperidine-1-carboxamide		-145.795	-6.93168
22	164160974	(2R,3S)-2-[3-[6-methyl-3-(1H-pyrazol-4-yl)indazol-1-yl]propyl]piperidin-3-ol		-145.773	-5.5413
23	71588244	1-[[2-(cyclopropane carbonylamino)phenyl]methyl]indazole-3-carboxamide		-145.705	-4.35413
24	126900931	1-[1-(1-methylindazole-3-carbonyl)azetidin-3-yl]pyrazole-4-carboxamide		-145.601	-5.14737
25	128980136	1-ethyl-3-[[[(2S,4R)-4-methoxy-2-(4-methyl-1,2,4-triazol-3-yl)pyrrolidin-1-yl]methyl]indazole		-145.422	-3.02409

DFG (Asp-Phe-Gly) are the first three amino acid residues that form an activation loop in the catalytic site of SRC kinase, depending on the direction the aspartate residue is oriented; it has two distinct conformations known as DFG-in and DFG-out. When it comes to catalysis, it indicates whether or not the aspartate can bind magnesium ions. These are referred to as the active and inactive conformations of the enzyme, respectively. In addition to the DFG motif's conformation, there is also the α -C conformation, which is defined as

either α -C-in or α -C-out depending on whether the salt bridge occurs between α C-glutamate and β 3-lysine. However, SRC kinase has a unique inactive conformation that is also known as DFG-intermediate conformation, with aspartate residue folding inside and α -C-out. The hinge region is made up of glutamate-339, tyrosine-340, methionine-341, serine-345, lysine-343, and glycine-344 residues [34]. Overall, along with the amino acid residues of the hinge region, the Asp-Phe-Gly triad of the DFG motif is the crucial set of

amino acids to take into account for the investigation of the interaction with docked ligands. Binding site interactions of pyrazole analogs revealed that most of the pyrazole analogs showed interactions with the DFG motif, Asp-404, Phe-405, and Gly-406 except 57122893, and 79300032, which showed interaction only with Asp-404, Phe-405. In the case of indazole and imidazopyridine analogs, all of them have shown interaction with the DFG motif. In the hinge region, around 18 pyrazole analogs about the same number of indazole and imidazopyridine analogs showed interactions with

Glu-339, and very few, only 4 pyrazole analogs interacted with Tyr-340 and Met-341, but in the case of indazole, and imidazopyridine analogs, around 15 analogs have shown interactions. Most analogs from both classes have shown interaction with Thr-338, the gatekeeper residue. It is a highly conserved residue that controls the access of inhibitors to the hydrophobic cavity not contacted by ATP within the ATP binding site, and it confers the selectivity and binding affinity of the inhibitors [35].

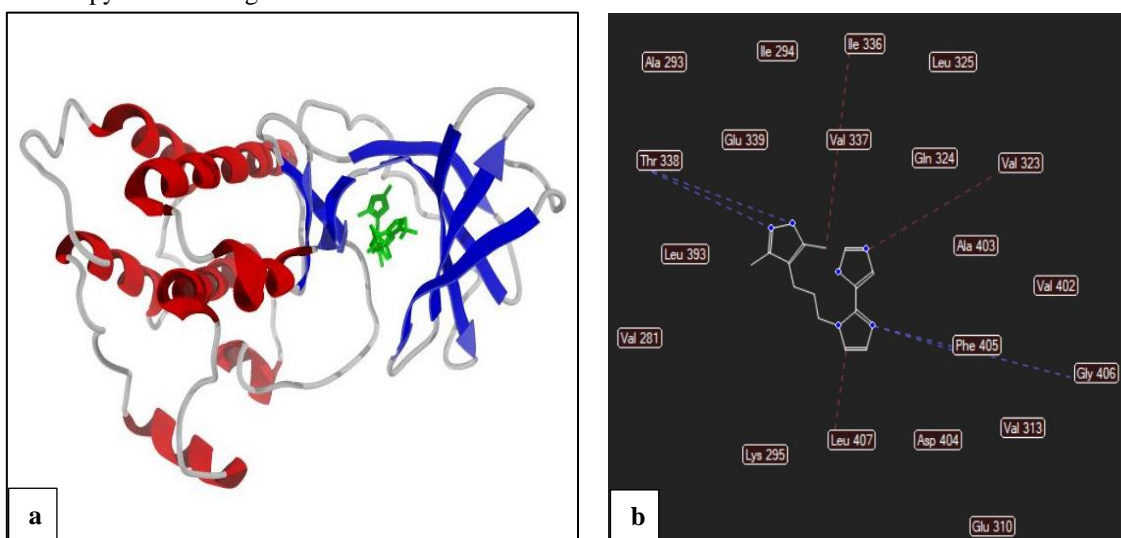


Figure 2. Orientation of 70736676 in the binding pocket of 6L8L in 3D (a) and interaction with amino acid residues in 2D (b). Blue dotted lines indicate H-bond and red dotted lines indicate steric interactions.

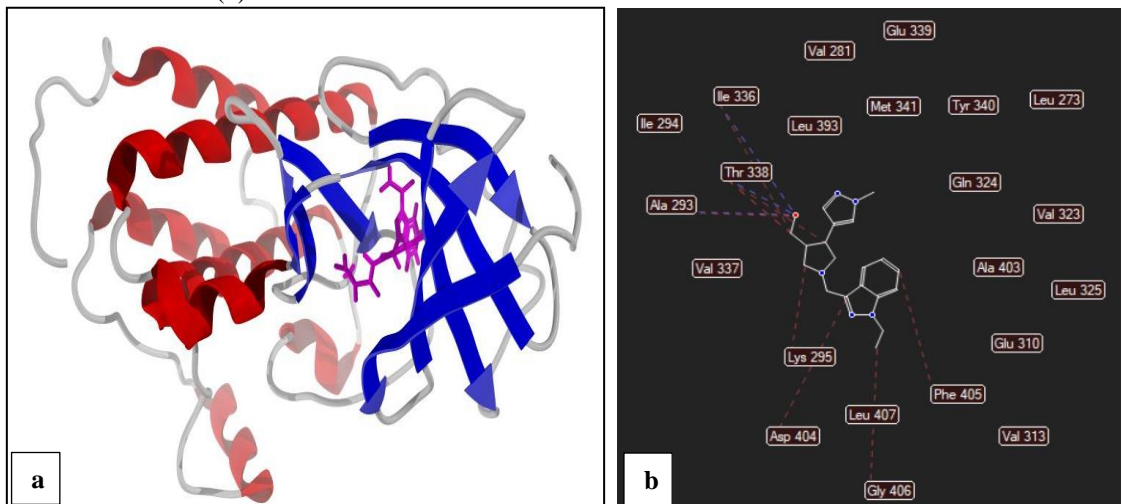


Figure 3. Orientation of 71588244 in the binding pocket of 6L8L in 3D (a) and interaction with amino acid residues in 2D (b). Blue dotted lines indicate H-bond and red dotted lines indicate steric interactions.

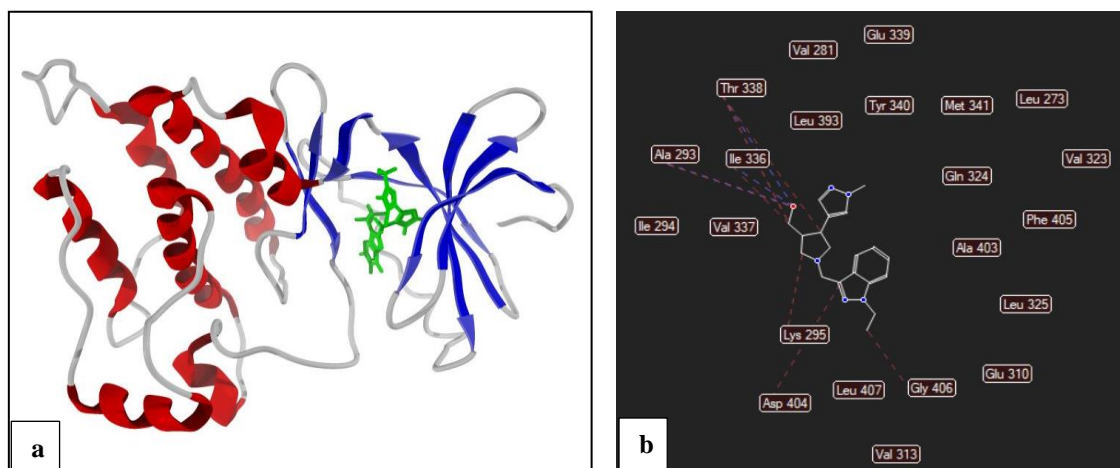


Figure 4. Orientation of 22380093 in the binding pocket of 6L8L in 3D (a) and interaction with amino acid residues in 2D (b). Blue dotted lines indicate H-bond and red dotted lines indicate steric interactions.

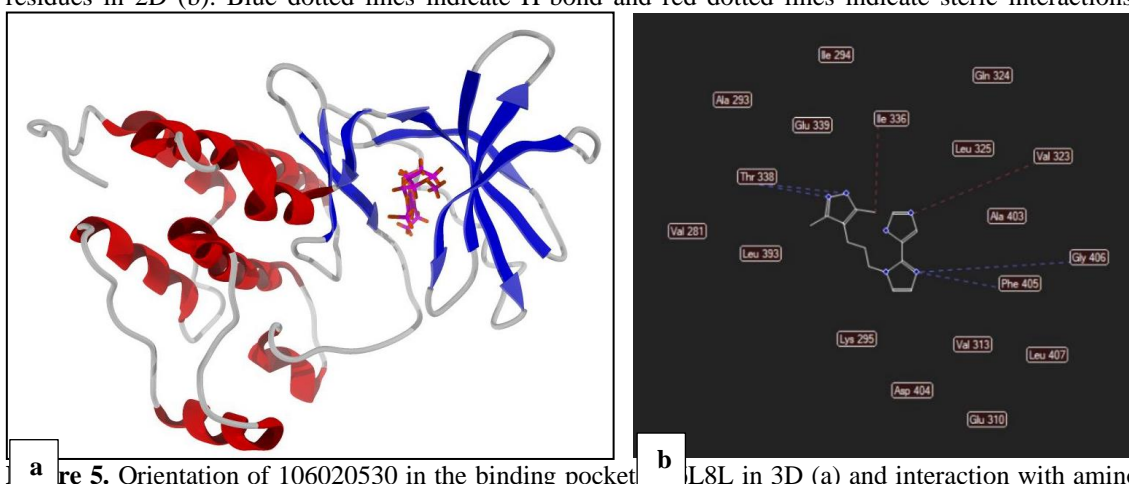


Figure 5. Orientation of 106020530 in the binding pocket of 6L8L in 3D (a) and interaction with amino acid residues in 2D (b). Blue dotted lines indicate H-bond and red dotted lines indicate steric interactions.

All of them exhibited strong H-bond interactions with Asp-404 and Phe-405, two residues of the DFG motif, and weak interactions were observed with Gly-406, the third residue of the DFG motif. With the Thr-338 residue, H-bond interactions are there with almost all the ligands. Other commonly observed interactions with variable energies were with Lys-295, Leu-393, Ile-336, and Ala-403,

which are all part of the SH1 catalytic domain. In the hinge region, just a few of the analogs interacted with extremely weak hydrophobic forces. No significant H-bond interactions were seen at the hinge region. Interactions of the top 25 ligands in each class have been given in Table 4 and energy details are given in supplementary material.

Table 4. List of amino acids interacting with the top 25 ligands in both sets that have shown the best binding energy

Sl. No.	PubChem Id	Amino acid residues	Sl. No.	PubChem Id	Amino acid residues
1	70736676	Gly-406, Phe-405, Asp-404, Glutamate-339, Lys-295, Ile-336 and Thr-338	26	22380154	Gly-406, Phe-405, Asp-404, Lys-295, Ile-336 and Thr-338
2	106405701	Gly-406, Phe-405, Asp-404, Glutamate-339, and Thr-338	27	22380093	Gly-406, Phe-405, Asp-404, Glutamate-339, Tyrosine-340, Methionine-341, Lys-295, Ile-336 and Thr-338

Rashmi P, Vishak Harish

Table 4. List of amino acids interacting with the top 25 ligands in both sets that have shown the best binding energy

Sl. No.	PubChem Id	Amino acid residues	Sl. No.	PubChem Id	Amino acid residues
3	56861793	Gly-406, Phe-405, Asp-404, Lys-295, Ile-336 and Thr-338	28	120602685	Gly-406, Phe-405, Asp-404, Glutamate-339, Tyrosine-340, Methionine-341, Lys-295, Ile-336 and Thr-338
4	4768943	Gly-406, Phe-405, Asp-404, Glutamate-339, Tyrosine-340, Methionine-341, Lys-295, Ile-336 and Thr-338	29	142663274	Gly-406, Phe-405, Asp-404, Lys-295, Ile-336 and Thr-338
5	156321592	Gly-406, Phe-405, Asp-404, Glutamate-339, Lys-295, Ile-336 and Thr-338	30	137968568	Gly-406, Phe-405, Asp-404, Lys-295, Ile-336 and Thr-338
6	91772399	Gly-406, Phe-405, Asp-404, Glutamate-339, Tyrosine-340, Methionine-341, Lys-295, Ile-336 and Thr-338	31	136102669	Gly-406, Phe-405, Asp-404, Glutamate-339, Tyrosine-340, Lys-295, Ile-336 and Thr-338
7	106020530	Gly-406, Phe-405, Asp-404, Glutamate-339, Lys-295, Ile-336 and Thr-338	32	120431098	Gly-406, Phe-405, Asp-404, Glutamate-339, Tyrosine-340, Methionine-341, Lys-295, Ile-336 and Thr-338
8	104447491	Gly-406, Phe-405, Asp-404, Glutamate-339, Lys-295, Ile-336 and Thr-338	33	22380098	Gly-406, Phe-405, Asp-404, Glutamate-339, Tyrosine-340, Methionine-341, serine-345, lysine-343, and glycine-344
9	135966420	Gly-406, Phe-405, Asp-404, and Lys-295, Ile-336 and Thr-338	34	72859965	Gly-406, Phe-405, Asp-404, Glutamate-339, Tyrosine-340, Methionine-341, serine-345, lysine-343, and glycine-344
10	41709670	Gly-406, Phe-405, Asp-404, Glutamate-339, Tyrosine-340, Methionine-341, Lys-295, Ile-336 and Thr-338	35	137865110	Gly-406, Phe-405, Asp-404, Glutamate-339, Tyrosine-340, Methionine-341, Lys-295, Ile-336 and Thr-338
11	84206551	Gly-406, Phe-405, Asp-404, Glutamate-339, Lys-295, Ile-336 and Thr-338	36	22380297	Gly-406, Phe-405, Asp-404, Glutamate-339, Tyrosine-340, Methionine-341, Ser-345, Lys-295, Ile-336 and Thr-338
12	119066539	Gly-406, Phe-405, Asp-404, Glutamate-339, Lys-295, Ile-336 and Thr-338	37	24738083	Gly-406, Phe-405, Asp-404, Glutamate-339, Tyrosine-340, Methionine-341, Serine-345, Lys-295, Ile-336 and Thr-338
13	115990819	Gly-406, Phe-405, Asp-404, Glutamate-339 Lys-295, Ile-336 and Thr-338	38	128979665	Gly-406, Phe-405, Asp-404, Glutamate-339, serine-345, lysine-343, and glycine-344
14	126947450	Gly-406, Phe-405, Asp-404, Glutamate-339, Lys-295 and Thr-338	39	166048341	Gly-406, Phe-405, Asp-404, Glutamate-339, Lys-295, Ile-336 and Thr-338
15	90935652	Gly-406, Phe-405, Asp-404, Glutamate-339, Lys-295, Ile-336 and Thr-338	40	20812083	Gly-406, Phe-405, Asp-404, Glutamate-339, Tyrosine-340, Methionine-341, Lys-295, Ile-336 and Thr-338

Table 4. List of amino acids interacting with the top 25 ligands in both sets that have shown the best binding energy

Sl. No.	PubChem Id	Amino acid residues	Sl. No.	PubChem Id	Amino acid residues
16	129327913	Gly-406, Phe-405, Asp-404, Glutamate-339, Lys-295, Ile-336 and Thr-338	41	128976367	Gly-406, Phe-405, Asp-404, Lys-295, Ile-336 and Thr-338
17	79288542	Gly-406, Phe-405, Asp-404, Glutamate-339, Lys-295, Ile-336 and Thr-338	42	20812061	Gly-406, Phe-405, Asp-404, Glutamate-339, Tyrosine-340, Lys-295, Ile-336 and Thr-338
18	60924396	Gly-406, Phe-405, Asp-404, Lys-295, Lys-295, Ile-336 and Thr-338	43	20812045	Gly-406, Phe-405, Asp-404, Glutamate-339, Tyrosine-340, Methionine-341, Lys-295, Ile-336 and Thr-338
19	79300032	Gly-406, Phe-405, Asp-404, Glutamate-339, Tyrosine-340, Methionine-341, Lys-295, Ile-336 and Thr-338	44	122107656	Gly-406, Phe-405, Asp-404, Glutamate-339, Tyrosine-340, Lys-295, Ile-336 and Thr-338
20	79307329	Gly-406, Phe-405, Asp-404, Glutamate-339, Lys-295, Ile-336 and Thr-338	45	146126560	Gly-406, Phe-405, Asp-404, Glutamate-339, Tyrosine-340, Methionine-341, serine-345, Lys-295, Ile-336 and Thr-338
21	57122893	Gly-406, Phe-405, Asp-404, Glutamate-339, Tyrosine-340, Methionine-341, Lys-295, Ile-336 and Thr-338	46	72865216	Gly-406, Phe-405, Asp-404, Glutamate-339, Tyrosine-340, Methionine-341, serine-345, lysine-343, and glycine-344
22	132318830	Gly-406, Phe-405, Asp-404, Glutamate-339, Lys-295, Ile-336 and Thr-338	47	164160974	Gly-406, Phe-405, Asp-404, Glutamate-339, Lys-295, Ile-336 and Thr-338
23	116630266	Gly-406, Phe-405, Asp-404, Lys-295 and Thr-338	48	71588244	Gly-406, Phe-405, Asp-404, Lys-295, Ile-336 and Thr-338
24	60509598	Gly-406, Phe-405, Asp-404, Glutamate-339, Tyrosine-340, Methionine-341, Lys-295, Ile-336 and Thr-338	49	126900931	Gly-406, Phe-405, Asp-404, Glutamate-339, Tyrosine-340, Methionine-341, Ser-345, Lys-295, Ile-336 and Thr-338
25	116864159	Gly-406, Phe-405, Asp-404, Lys-295, Ile-336 and Thr-338	50	128980136	Gly-406, Phe-405, Asp-404, Glutamate-339, Tyrosine-340, Methionine-341, Lys-295, Ile-336 and Thr-338

3.2. ADMET studies

Drug discovery is a lengthy process characterized by significant research expenses. High costs often result from failures rather than successful outcomes. Several drug candidates are unsuccessful in pre-clinical or clinical trials due to safety concerns that can be attributed to inadequate absorption, distribution, metabolism, excretion, and toxicity (ADMET) profiles. ADMET studies evaluate how a drug interacts with different physiological activities in the body. ADMET studies are essential for examining a drug's impact

on the entire human system, as well as the body's impacts on the drug, omitting the target location. Examining and improving ADME qualities at the initial phases of drug development is essential for the effectiveness and safety of the drug candidate, as it offers vital insights about the drug's behavior in a biological environment. In in-silico ADMET studies, we can analyze the impact of the drug in the biological system using the databases where ADMET data associated with particular structures/fragments is available. These databases are used to predict the effect of ADMET

Rashmi P, Vishak Harish

characteristics of new lead drugs in humans by using data from animal in vivo ADMET research. About 100 pyrazole analogs and 100 indazole and imidazopyridine analogs together were subjected to ADMET screening.

Drugs need to achieve a particular concentration at the active site to elicit a biological response, which is influenced by the rate of absorption. Orally administered drugs must pass through the cell membranes of the intestines. Caco-2 cells, derived from human colon adenocarcinoma, are utilized as an alternative for human intestinal epithelium in research. Caco-2 cells are utilized for assessing the permeability of lead compounds, and Caco-2 permeability serves as a crucial indicator for potential therapeutic candidates. Caco-2 cells are utilized for assessing the permeability of lead compounds, and Caco-2 permeability serves as a crucial indicator for potential therapeutic candidates. The majority of pyrazole (70%), indazole, and imidazopyridine analogs were predicted to have good oral absorption based on the results of caco-2 permeability. Those with poor oral absorption can be tried for different routes of absorption other than the oral route.

For a drug to be effective, it must rapidly distribute in the body at the required concentration following absorption. Several drug candidates bind to plasma proteins in the blood, decreasing the quantity of free drug available and influencing pharmacodynamics. Ideal pharmacodynamic behavior requires optimal plasma protein binding for any drug candidate. Around 50 % of pyrazole analogs exhibit protein binding ranging from 70 % to 90 %, which is acceptable. Around 50 % of indazole, and imidazopyridine analogs are also favorable, but in the range of 70 % to 90 %. The rest exhibit protein binding exceeding 90 %, which is considered undesirable.

Another crucial consideration is whether a drug can penetrate the Blood-Brain Barrier (BBB) but current lead molecules should not cross BBB. Nearly 60 % of pyrazole analogs are predicted to have the probability of crossing BBB, whereas in the case of indazole and imidazopyridine analogs have 80%. This signifies the likelihood of side effects on the central nervous system.

The volume of distribution is an essential factor that relates the initial drug dose to its initial concentration in the systemic circulation, in

addition to the other mentioned parameters. A volume of distribution ranging from 0.04 to 20 L/Kg is considered acceptable. All ligands of pyrazole, indazole, and imidazopyridines fall within an acceptable range for volume of distribution.

Metabolism, also known as biotransformation, is essential for rapid drug detoxification and for activating prodrugs. Metabolic rate influences both the drug's duration of action and its elimination process. Phase I of metabolic reactions involves oxidative processes, while phase II involves conjugative reactions. The human cytochrome P450 family has 57 isozymes that participate in the majority of phase I metabolic reactions and are responsible for the metabolism of most drugs and drug candidates. Enzymes 2D6, 3A4, 1A2, 2C19, and 2C9 are used to predict the metabolism of potential drug candidates on a scale from 0 to 1. Pyrazole, Indazole, and imidazopyridine analogs are expected to act as substrates or inhibitors of Cytochrome P450 isoforms 2D6, 3A4, 1A2, 2C19, and 2C9 based on their values falling within the range that suggests they could function as inhibitors or substrates.

It is essential to eliminate the drug and its metabolites to avoid their accumulation, which can result in further complications. The solubility of the drug and its metabolites is a contributing factor in excretion. Clearance and half-life are the key parameters used to evaluate the excretion of drug candidates. Both are interrelated with each other and with the volume of distribution influencing the dosage frequency. 80% of pyrazole analogs have shown greater clearance with values over 5 ml/min/kg. 10-15% are expected to have a favorable half-life ranging from 0 to 0.3, while approximately 50% are anticipated to have a poor half-life, with the remaining showing an average half-life. Around 25% to 30% of indazole and imidazopyridine analogs are expected to have a poor half-life, the rest falling within the range of good to average, while 80% to 90% show better clearance. All the results of the ADMET screening are given in supplementary material.

Drugs may have adverse effects due to toxicity in particular organs or some drugs may be toxic based on the dose. We must analyze the toxicity levels to minimize the impact. Various toxicity parameters are considered for evaluation. The hERG (cardiac

Rashmi P, Vishak Harish

potassium channel encoded by the human ether-a-go-go-related gene) toxicity is a significant parameter widely considered due to its potential to cause arrhythmia, long QT syndrome that may lead to fainting or sudden death. The other significant toxicity indicators considered are human hepatotoxicity (H-HT), Drug-induced liver injury (DILI), skin sensitization, carcinogenicity, and respiratory toxicity.

Most Pyrazole, indazole, and imidazopyridine analogs do not exhibit hERG toxicity, with only a small number of ligands showing such effects. Only 4-5 pyrazole molecules and nearly 10% of indazole and imidazole analogs have exhibited skin sensitivity. Nonetheless, nearly 65% of pyrazole, indazole, and imidazopyridine analogs are expected to be hepatotoxic, with 75% anticipated to cause drug-induced liver injury. Nearly forty to forty-five percent of pyrazole molecules, as well as 70-75 percent of indazole and imidazopyridine analogs, have been shown to be carcinogenic, with 70% to 75% of pyrazol, indazole, and imidazopyridine analogs expected to be respiratory toxic. Anti-cancer drugs are commonly known to cause respiratory, hepatotoxicity, and hERG toxicity [36,

37]. Carcinogenicity is also an important factor to consider. In summary, all three classes of molecules are safe in terms of hERG toxicity, but we expect the majority to be toxic in terms of respiratory toxicity and carcinogenicity. In the case of drug-induced liver damage and hepatotoxicity, the majority of all three ligand classes were predicted to be toxic. Identifying completely non-toxic compounds within the three classes was extremely challenging; however, we consider ligand molecules that do not exhibit hERG, respiratory toxicity, skin sensitivity, or carcinogenicity as the least toxic, as shown in Table 5. Such molecules are chosen from all three classes, with pyrazoles and indazoles accounting for the majority of them. The majority of imidazopyridine did not meet our criteria and was predicted to show one or more of the four toxicities categories that we considered.

The ligands with the highest binding affinity and least toxicity (absence of respiratory toxicity, skin sensitivity, or carcinogenicity) were selected individually for molecular dynamics (MD) simulations to study the behavior and interactions between the protein and ligand in close proximity.

Table 5. Selected compounds predicted to be least toxic and their toxicities

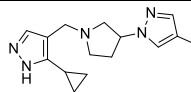
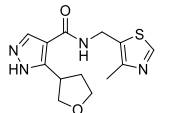
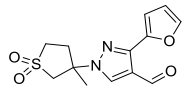
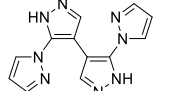
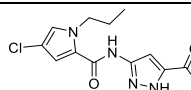
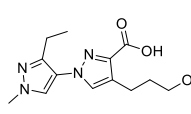
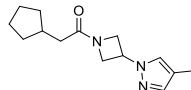
Sl. No.	PubChem Id	IUPAC Name	Structure	hERG ^a	H-HT ^a	DILI ^a	SS	Car ^a	RT
1	126947450	1-[1-[(5-cyclopropyl-1H-pyrazol-4-yl)methyl]pyrrolidin-3-yl]-4-methylpyrazole		0.436	0.811	0.961	0.317	0.156	0.34
2	128968081	N-[(4-methyl-1,3-thiazol-5-yl)methyl]-5-(oxolan-3-yl)-1H-pyrazole-4-carboxamide		0.061	0.614	0.967	0.094	0.034	0.037
3	60924396	3-(furan-2-yl)-1-(3-methyl-1,1-dioxothiolan-3-yl)pyrazole-4-carbaldehyde		0.019	0.723	0.956	0.041	0.449	0.178
4	57122893	5-pyrazol-1-yl-4-(5-pyrazol-1-yl-1H-pyrazol-4-yl)-1H-pyrazole		0.062	0.465	0.998	0.042	0.049	0.274
5	64527682	3-[(4-chloro-1-propylpyrrole-2-carbonyl)amino]-1H-pyrazole-5-carboxylic acid		0.031	0.831	0.986	0.04	0.03	0.214
6	107463827	1-(3-ethyl-1-methylpyrazol-4-yl)-4-(3-hydroxypropyl)pyrazole-3-carboxylic acid		0.02	0.487	0.989	0.045	0.478	0.096
7	126900899	1-[1-(2-cyclopentylacetyl)azetidin-3-yl]pyrazole-4-carboxamide		0.032	0.862	0.855	0.106	0.433	0.013

Table 5. Selected compounds predicted to be least toxic and their toxicities

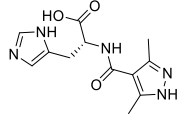
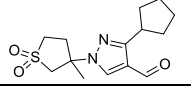
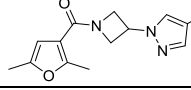
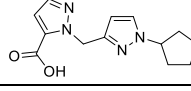
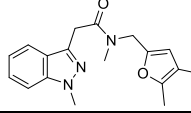
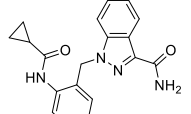
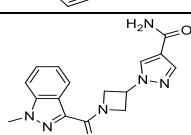
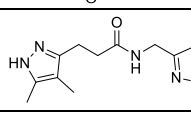
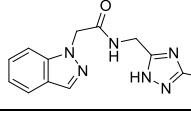
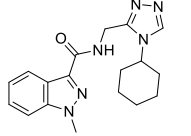
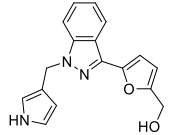
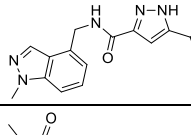
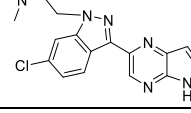
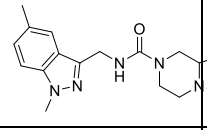
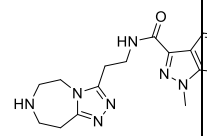
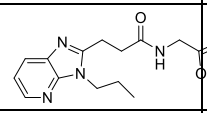
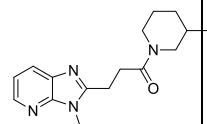
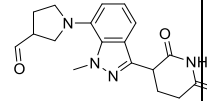
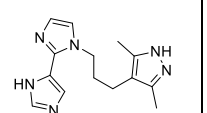
Sl. No.	PubChem Id	IUPAC Name	Structure	hERG ^a	H-HT ^a	DILI ^a	SS	Car ^a	RT
8	104894301	(2R)-2-[(3,5-dimethyl-1H-pyrazole-4-carbonyl)amino]-3-(1H-imidazol-5-yl)propanoic acid		0.053	0.772	0.968	0.123	0.024	0.143
9	62631909	3-cyclopentyl-1-(3-methyl-1,1-dioxothiolan-3-yl)pyrazole-4-carbaldehyde		0.014	0.603	0.951	0.059	0.492	0.65
10	126900490	1-[1-(2,5-dimethylfuran-3-carbonyl)azetidin-3-yl]pyrazole-4-carbonitrile		0.027	0.97	0.976	0.075	0.948	0.01
11	64784375	2-[(1-cyclopentylpyrazol-3-yl)methyl]pyrazole-3-carboxylic acid		0.031	0.501	0.984	0.082	0.033	0.021
12	122107656	2-methyl-5-[[methyl-[2-(1-methylindazol-3-yl)acetyl]amino]methyl]furan-3-carboxylic acid		0.025	0.301	0.972	0.049	0.085	0.02
13	71588244	1-[[2-(cyclopropanecarbonylamino)phenyl]methyl]indazole-3-carboxamide		0.594	0.608	0.78	0.118	0.286	0.145
14	126900931	1-[1-(1-methylindazole-3-carbonyl)azetidin-3-yl]pyrazole-4-carboxamide		0.083	0.91	0.975	0.032	0.442	0.019
15	118779370	3-(4,5-dimethyl-1H-pyrazol-3-yl)-N-[(1-ethylindazol-3-yl)methyl]propanamide		0.04	0.714	0.382	0.065	0.147	0.323
16	91790722	2-indazol-1-yl-N-[(3-pyridin-4-yl-1H-1,2,4-triazol-5-yl)methyl]acetamide		0.057	0.623	0.982	0.066	0.506	0.52
17	131916416	N-[(4-cyclohexyl-1,2,4-triazol-3-yl)methyl]-1-methylindazole-3-carboxamide		0.049	0.657	0.371	0.038	0.381	0.331
18	21106977	[5-[1-(1H-pyrrol-3-yl)methyl]indazol-3-yl]furan-2-yl]methanol		0.217	0.222	0.957	0.079	0.053	0.115
19	146153675	5-(furan-2-yl)-N-[(1-methylindazol-4-yl)methyl]-1H-pyrazole-3-carboxamide		0.074	0.253	0.879	0.033	0.285	0.513
20	141364950	2-[6-chloro-3-(5H-pyrrolo[2,3-b]pyrazin-2-yl)indazol-1-yl]-N,N-dimethylacetamide		0.202	0.86	0.951	0.047	0.353	0.672

Table 5. Selected compounds predicted to be least toxic and their toxicities

Sl. No.	PubChem Id	IUPAC Name	Structure	hERG ^a	H-HT ^a	DILI ^a	SS	Car ^a	RT
21	124208325	N-[(1,5-dimethylindazol-3-yl)methyl]-3-oxo-5,6,8,8a-tetrahydro-1H-[1,3]oxazolo[3,4-a]pyrazine-7-carboxamide		0.104	0.861	0.217	0.084	0.24	0.017
22	56719975	1-methyl-N-[2-(6,7,8,9-tetrahydro-5H-[1,2,4]triazolo[4,3-d][1,4]diazepin-3-yl)ethyl]indazole-3-carboxamide		0.077	0.152	0.139	0.031	0.357	0.164
23	20867455	N-(furan-2-ylmethyl)-3-(3-propylimidazo[4,5-b]pyridin-2-yl)propanamide		0.094	0.114	0.278	0.116	0.644	0.647
24	56739074	3-(3-methylimidazo[4,5-b]pyridin-2-yl)-1-[3-(1H-pyrazol-5-yl)piperidin-1-yl]propan-1-one		0.067	0.658	0.164	0.098	0.207	0.652
25	167282363	1-[3-(2,6-dioxopiperidin-3-yl)-1-methylindazol-7-yl]pyrrolidine-3-carbaldehyde		0.014	0.634	0.188	0.508	0.264	0.054
26	70736676	4-[3-[2-(1H-imidazol-5-yl)imidazol-1-yl]propyl]-3,5-dimethyl-1H-pyrazole		0.08	0.902	0.921	0.64	0.022	0.92

SS: Skin Sensitivity^a

Car: Carcinogenicity^a

RT: Respiratory toxicity^a

a: Empirical values in the range of 0-0.3 considered as excellent, 0.3-0.7 as moderate and above as poor.

3.3. MD Simulations

To gain insight into the stability of the protein ligand complex, MD simulations for SRC kinase (PDB Id:6L8L) in complex with different ligands 4-[3-[2-(1H-imidazol-5-yl)imidazol-1-yl]propyl]-3,5-dimethyl-1H-pyrazole (PubChem Id: 70736676), 2-[[2-(4-chloro-1-methylpyrazol-3-yl)imidazol-1-yl]methyl]-3-(2-fluoroethyl)imidazo[4,5-b]pyridine (PubChem Id: 22380093), 1-[(1-ethylindazol-3-yl)methyl]-4-(1-methylpyrazol-4-yl)pyrrolidin-3-yl]methanol (PubChem Id: 120602685), that has shown best binding affinity, N-[(4-methyl-1,3-thiazol-5-yl)methyl]-5-[(3R)-oxolan-3-yl]-1H-pyrazole-4-carboxamide (PubChem Id:129327913), 1-[[2-(cyclopropane carbonylamino)phenyl]methyl]indazole-3-carboxamide (PubChem Id:71588244), those having least toxicity, 5-(chloromethyl)-3-ethyl-1-methyl-6-[(1-methylpyrrolidin-2-yl)methyl]imidazo[4,5-

c]pyrazole (PubChem Id: 106020530), 2-[[2-(2,5-dimethyl-1,3-dihydropyrazol-3-yl)imidazol-1-yl]methyl]-3-propyl imidazo[4,5-b]pyridine (PubChem Id: 142663274) having best ADME profile were performed for 25 ns under physiological conditions. MD simulation for the native ligand Ibrutinib along with SRC kinase has also been done for reference. The ligands were chosen in such a way that they exhibit least toxicity, better ADME profile and better binding affinity. The stability of the complexes was assessed using RMSD values. The RMSD graph of the native ligand Ibrutinib (Fig. 6h) shows that it began to stabilize at around 5 ns, but conformational changes occurred every 7 to 8 ns. Compound 70736676, a pyrazole analog, changed conformation very early but remained in the same conformation for the majority of the time, indicating relative stability (Fig. 6a). Compound 22380093 from imidazopyridine fluctuated and changed

Rashmi P, Vishak Harish

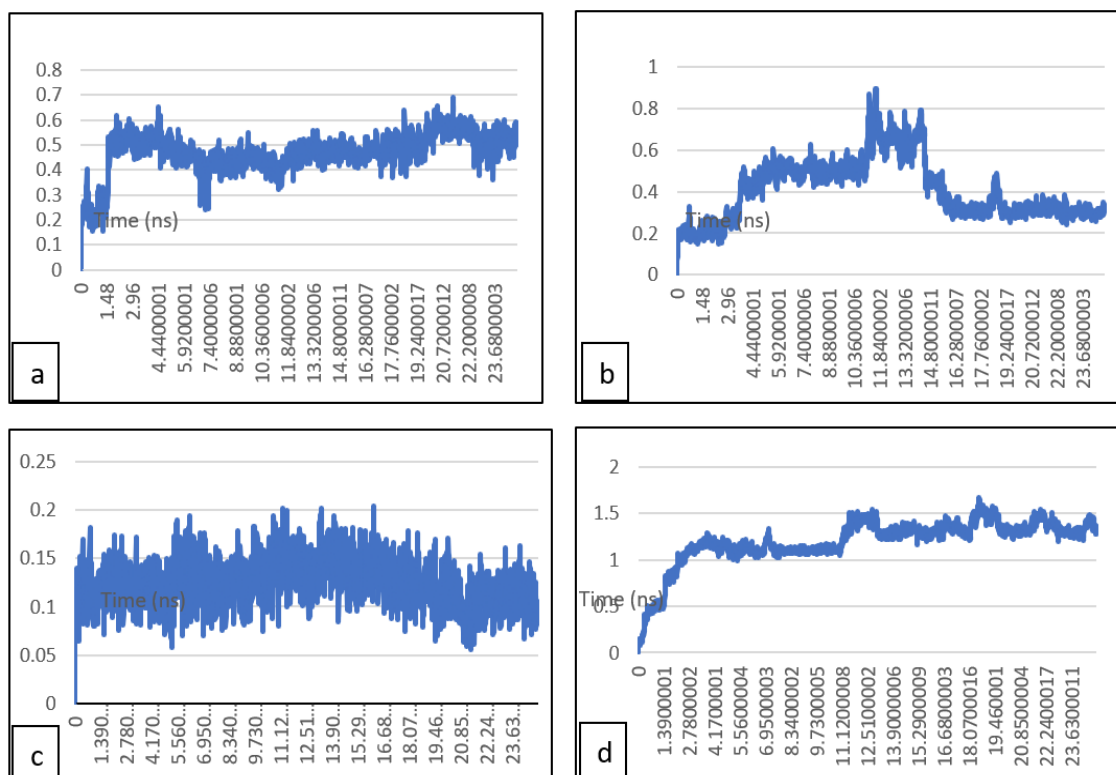
conformation before stabilizing at 19.25 ns (Fig. 6b). Compound 120602685, which has an indazole nucleus, changed conformation at 9.5 ns and remained stable for about 15 ns (Fig 6e). In the case of compound 129327913, RMSD gradually increased before stabilizing at 5.2, 10 ns (Fig 6f). The fluctuations were observed, and it was less stable. Compound 71588244 was found to be the most stable, with values ranging from 0.06 to 0.2 over 25 ns (Fig 6c). Compound 106020530 was very unstable, and many fluctuations were observed (Fig 6d). The compound 142663274 remained stable for 23 ns, but wobble was observed at the later stages (Fig 6g).

Root mean square fluctuation (RMSF) represents the flexible regions of a protein, with higher values indicating flexibility and lower values indicating rigidity. RMSF was applied to all 8 simulated systems depicted in the Fig 7. All eight systems showed a similar fluctuation pattern. The protein's terminal residues fluctuated the most. The overlapping of graphs obtained by RMSF values indicates that the fluctuations were almost similar among all complexes, as shown in Fig 7a & Fig 7b. Aside from that, flexibility was commonly

observed in the alpha helix region between Glu-339 and Tyr-376 in all systems. Overall, we observed fluctuations in Gly-465, Asn-468, Asp-518, and Phe-520.

The average RMSF values for SRC-Ibrutinib, SRC-70736676, SRC-129327913, SRC-106020530, SRC-120602685, SRC-142663274, SRC-71588244, and SRC-22380093 complexes were 0.109, 0.165, 0.155, 0.167, 0.145, 0.157, 0.133, and 0.163 nm, respectively. These results showed that all of the complexes were relatively stable. In comparison, the fluctuation in SRC-71588244 complex (Fig 7d) followed the same trend all other complexes (Figs 7d, 7e, and 7f), however the magnitude was lower. 71588244 could be considered best with minimal fluctuations.

The radius of gyration (Rg) reflects the compactness of the protein-ligand complex. When Rg values are low, it indicates that the molecule is compact or rigid, whereas high values indicate that the molecule has expanded. Rg values in MD simulations indicate the complex's stability throughout the process, including any changes in conformation or structure (Fig 8a & 8b).



Rashmi P, Vishak Harish

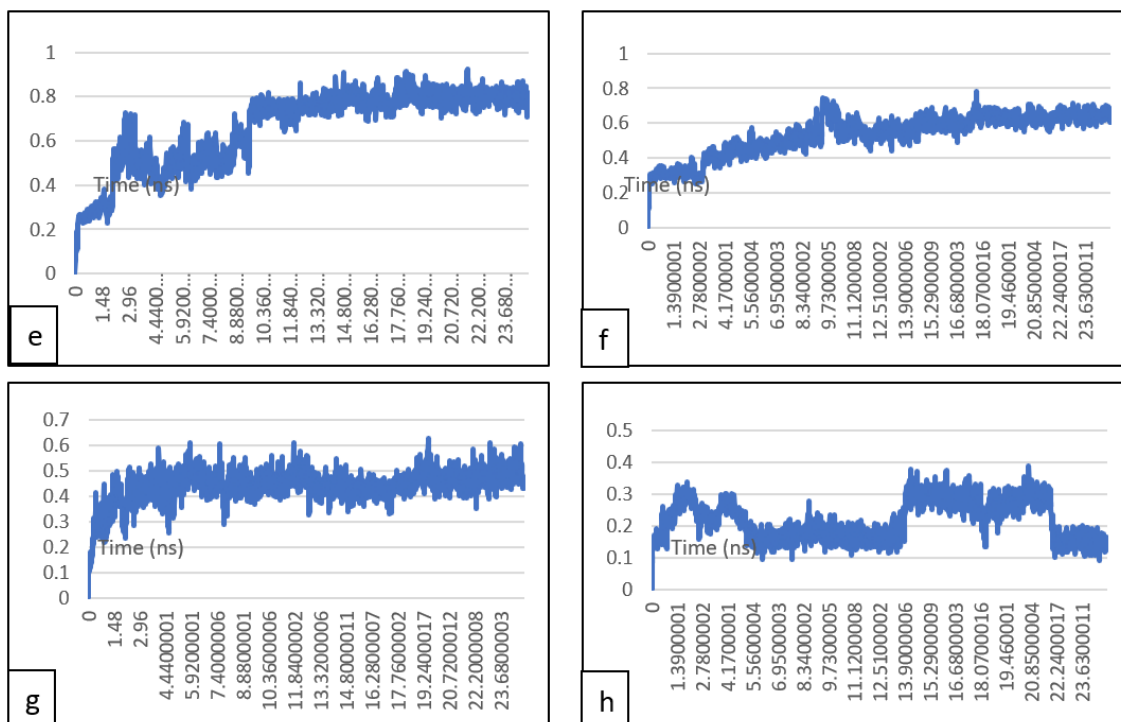
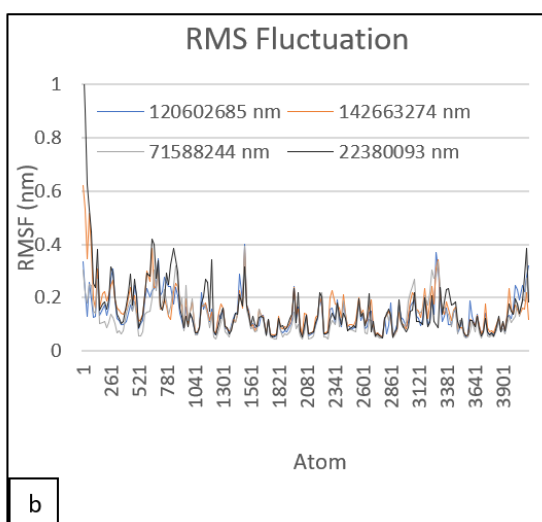
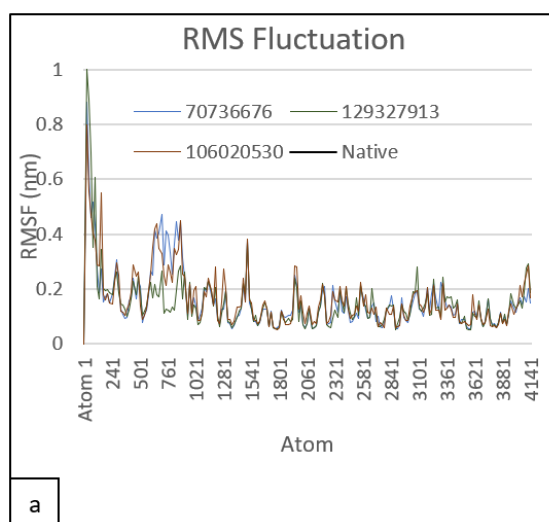


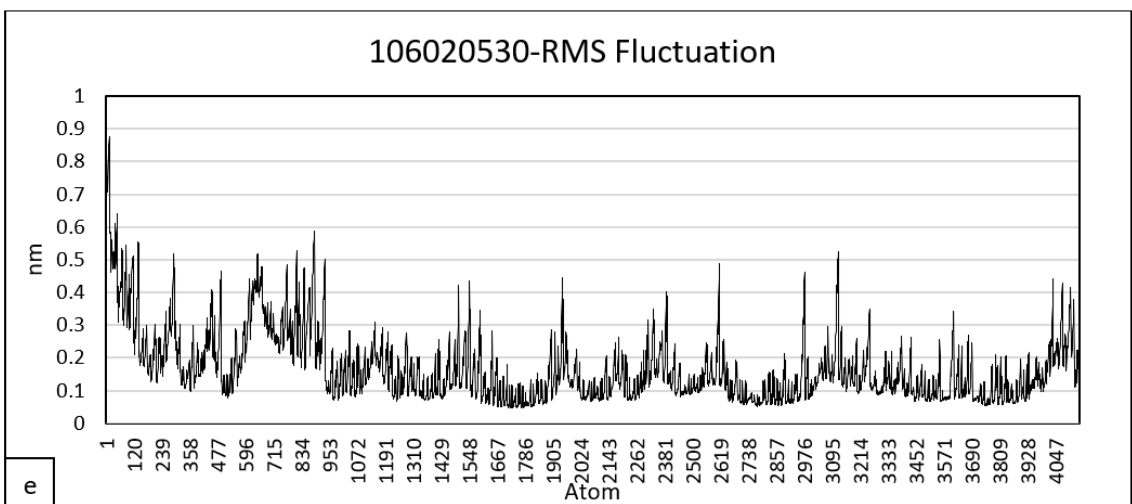
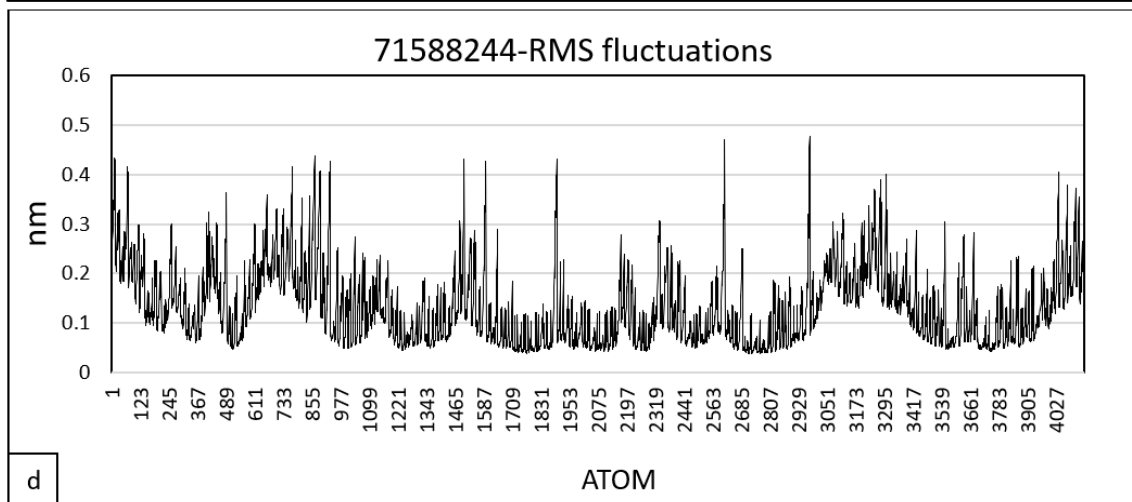
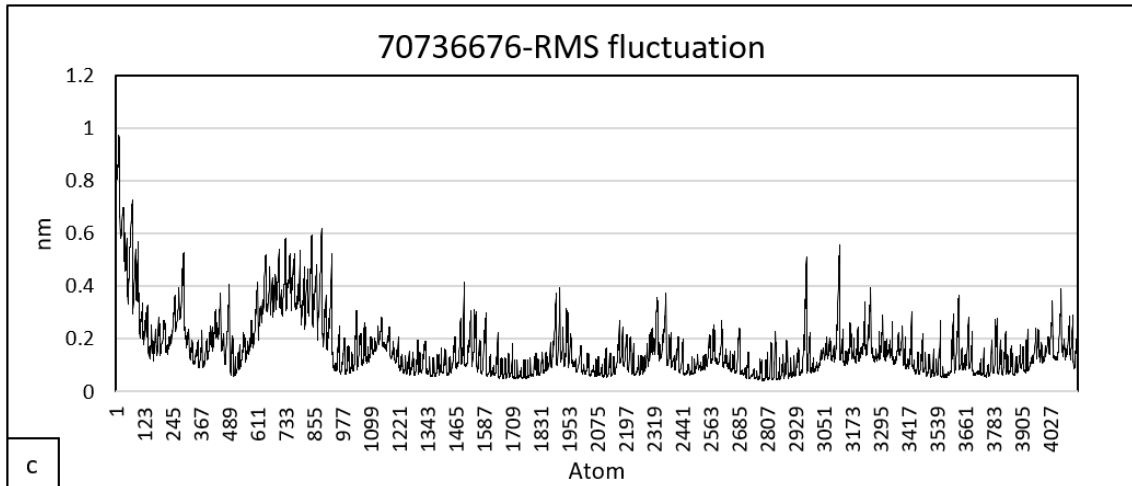
Figure 6. RMSD graphs of protein 6L8L in complex with seven selected ligands (a-g) and Ibrutinib, native ligand (h).

The 70736676-SRC complex exhibited slight variation within the range of 0.1 nm, but it remained stable and rigid throughout the process, with no indication of significant structural change (Fig 8c). Initially, the 129327913-SRC complex showed a slight change in structure; however, it became stable further, with variations falling within the range of 0.06 nm. The 106020530-SRC complex initially expanded in structure and became stable and rigid over time, as evidenced by decreasing values, and it remained stable with variations in the

range of 0.05 nm (Fig 8e). In the 120602685-SRC complex, and the 142663274-SRC complex, the structure initially relaxed before becoming stable in that position with variations of 0.1 nm. The 71588244-SRC complex initially exhibited variations; however, as time passed, the complex became rigid, with variations in the range of 0.04 nm (Fig 8d). The 22380093-SRC complex initially exhibited variations but became rigid after 13 ns, showing variations within the range of 0.05 nm (Fig 8f).



Rashmi P, Vishak Harish



Rashmi P, Vishak Harish

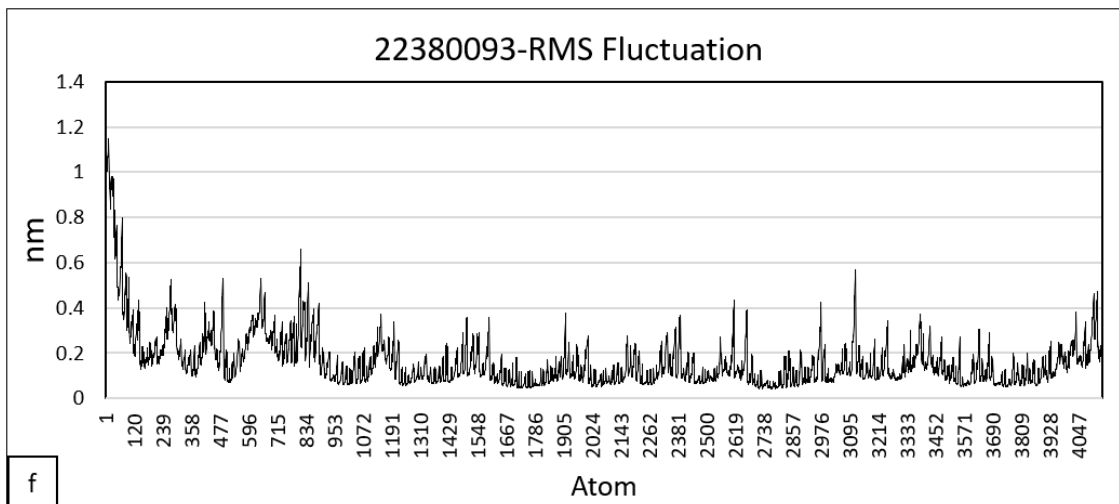
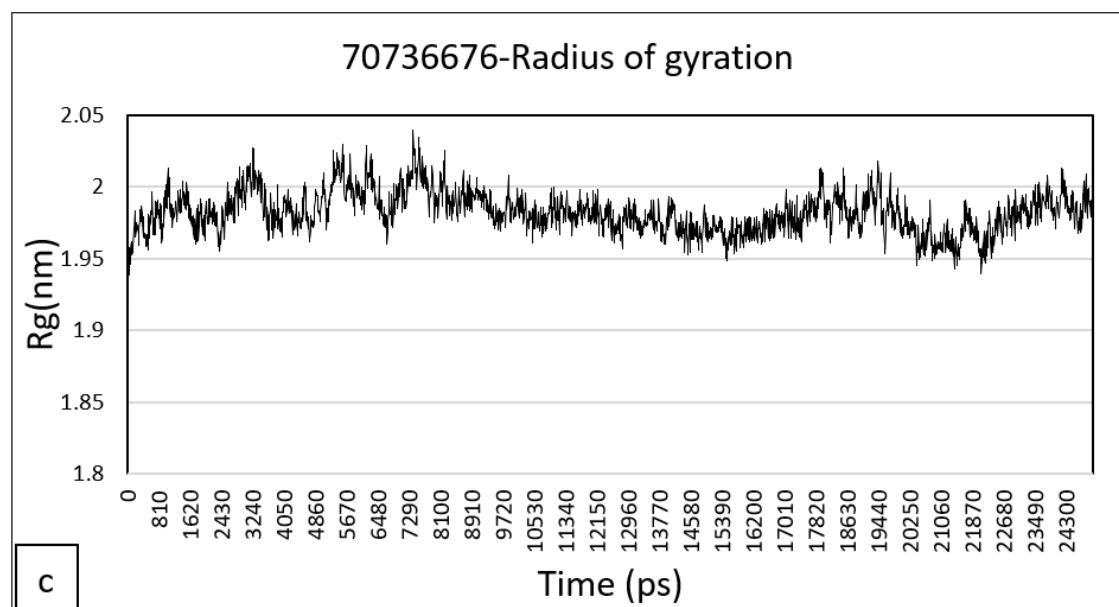
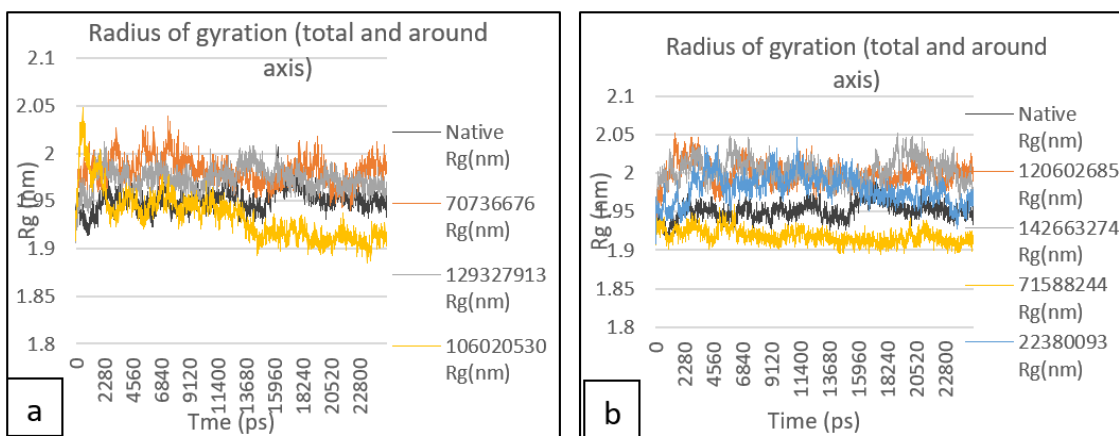


Figure 7. Overlap of RMSF values of 6L8L in complex with three ligands and native ligand ibrutinib in (a) and with four ligands in (b). RMS fluctuation of 70736676 (c), 71588244 (d), 106020530 (e), 22380093 (f).



Rashmi P, Vishak Harish

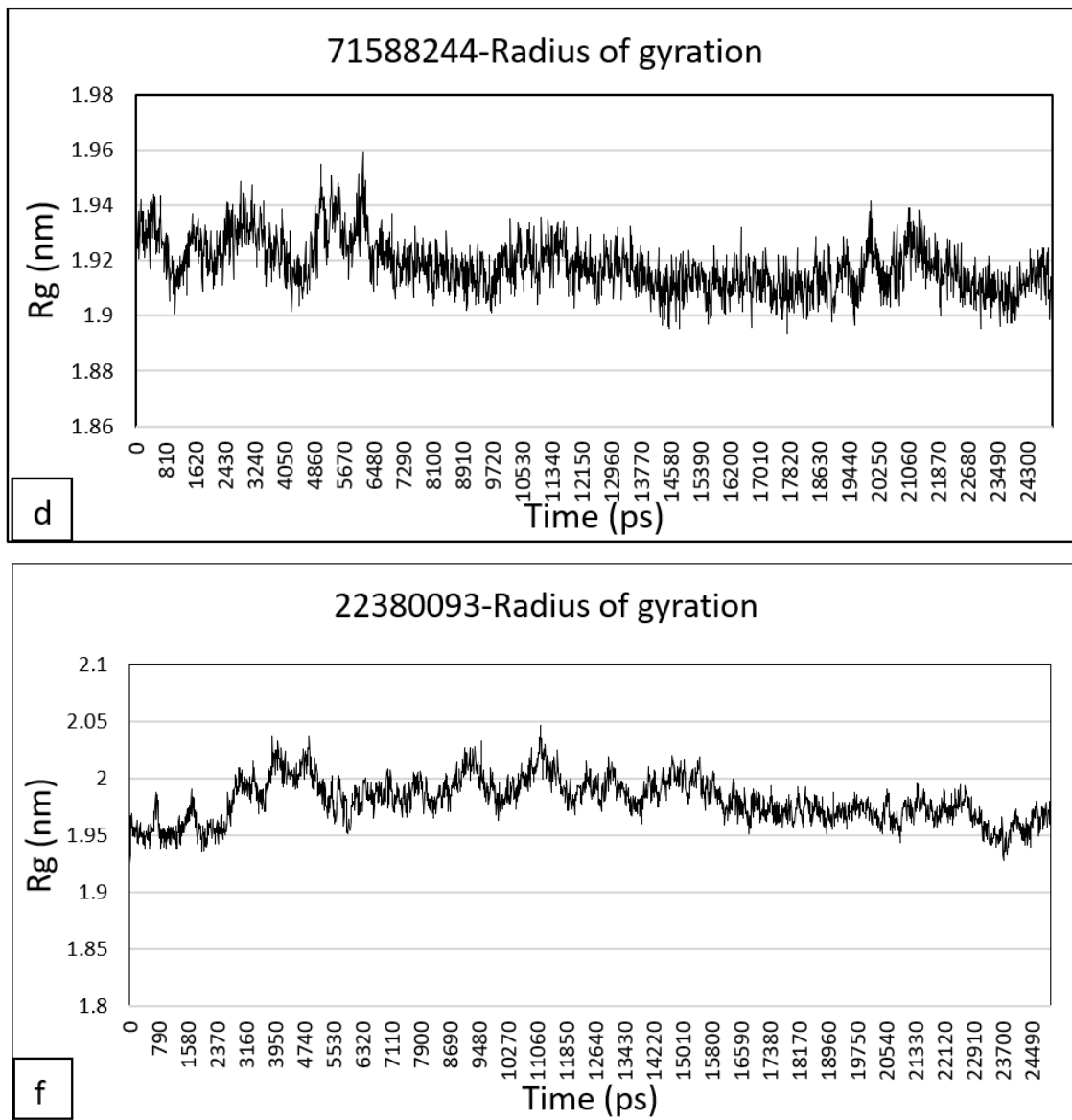
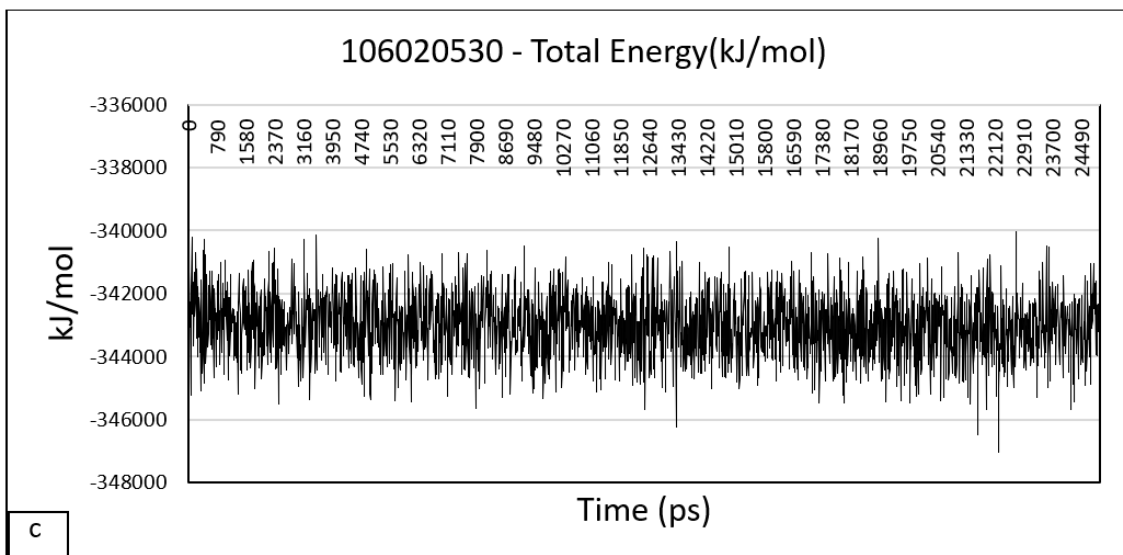
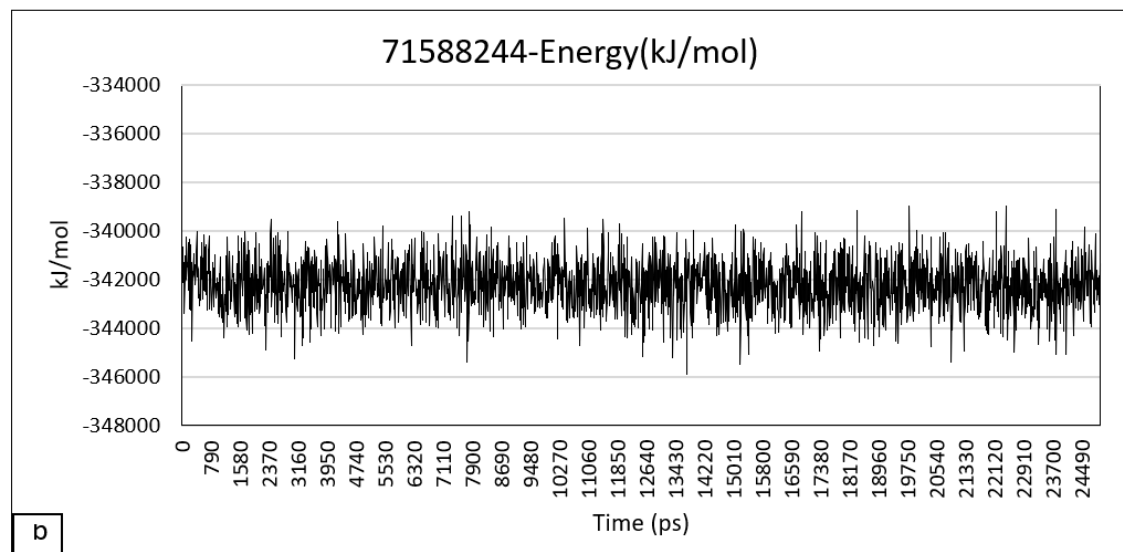
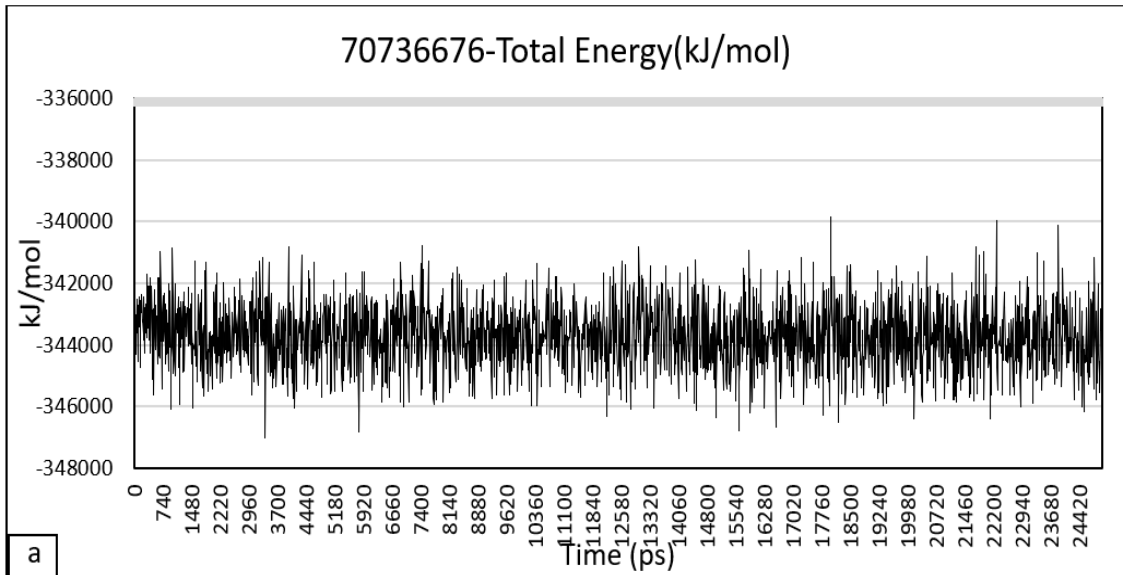


Figure 8. Overlap of Rg values of 6L8L in complex with three ligands and native ligand ibrutinib in (a) and with four ligands in (b). Radius of gyration of 70736676 (c), 71588244 (d), 106020530 (e), 22380093 (f).

Rashmi P, Vishak Harish



Rashmi P, Vishak Harish

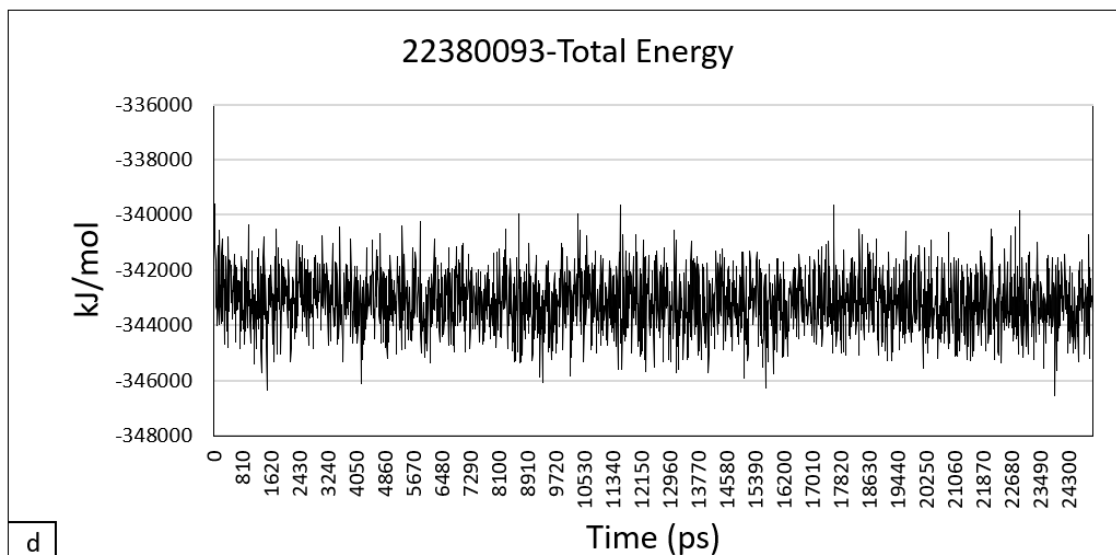


Figure 9. Graphs representing the total energy during MD simulation. a) Total energy graph of 70736676, b) Total energy graph of 71588244, c) Total energy graph of 106020530, d) Total energy graph of 22380093.

In comparison to standard Ibrutinib, the 71588244-SRC complex was more compact and rigid, whereas the 106020530-SRC complex became compact after 14 ns. The rest of the compounds were comparable to the standard Ibrutinib-SRC complex and could be considered useful.

The total energy which is the sum of potential energy and kinetic energy in the MD simulations is likely to be constant to ensure that the simulation is physically valid. Total energy of all complexes indicated that they were in equilibrium because

there were no systematic drifts in the value and only minor fluctuations (Fig 9a-Fig 9d).

H-bond analysis indicated that during the simulation, 71588244 showed four H-bonds, with at least three appearing the majority of the time. 70736676 showed 1-3 H bonds, with 2 appearing the majority of the time. 106020530 initially showed 1-2 H bonds, which later increased to three. The rest four of them showed 1-2 H bond interactions, but the majority of the time there were no H-bond interactions.

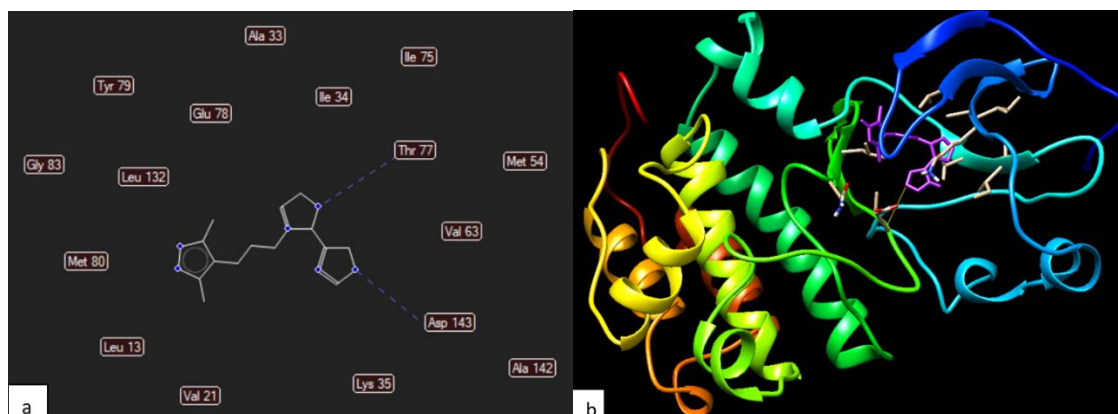


Figure 10. a) 2D diagram of the interaction of 70736676 with surrounding amino acids in the binding pocket of SRC kinase (PDB Id: 6L8L) during MD simulation. b) Binding mode of 70736676 in the binding pocket of SRC kinase (PDB Id: 6L8L) during MD simulation showing hydrogen bonding.

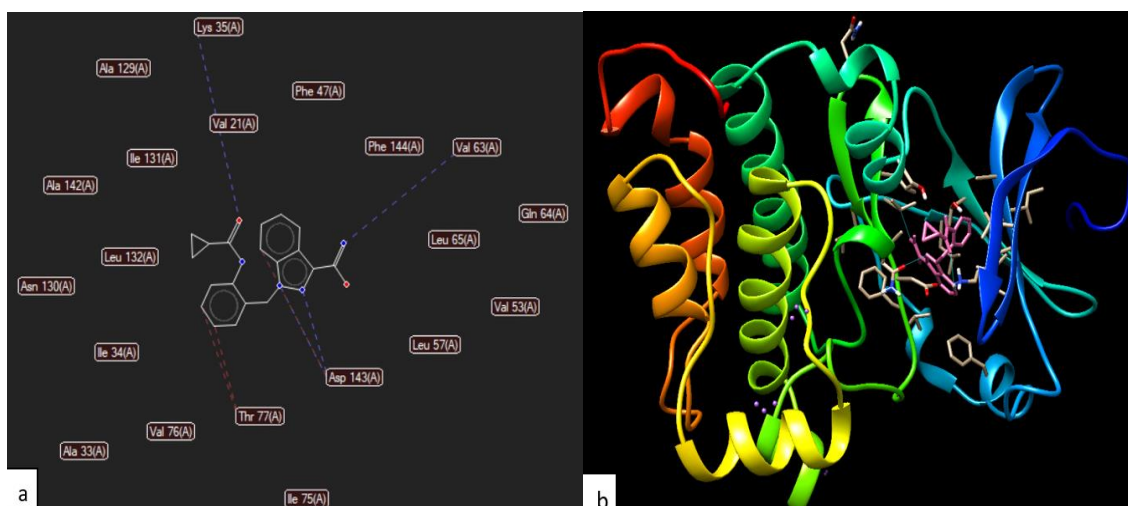


Figure 11. a) 2D diagram of the interaction of 71588244 with surrounding amino acids in the binding pocket of SRC kinase (PDB Id: 6L8L) during MD simulation. b) Binding mode of 71588244 in the binding pocket of SRC kinase (PDB Id: 6L8L) during MD simulation showing hydrogen bonding.

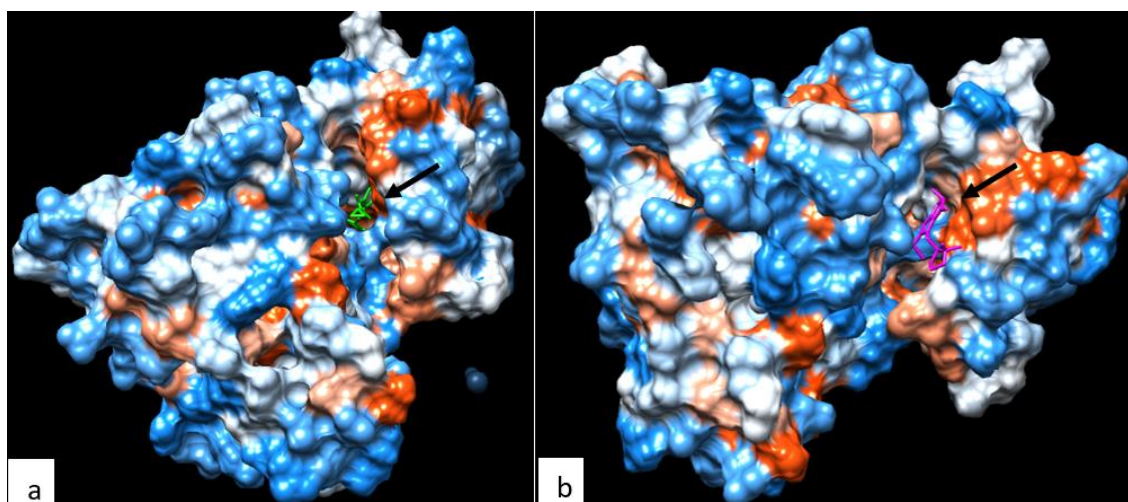


Figure 12. a) Visualization of electrostatic interaction of 71588244 in the binding pocket (light green color, position indicated with arrow) b) a) Visualization of electrostatic interaction of 106020530 in the binding pocket (purple color, position indicated with arrow)

During MD simulation it was observed that in spite of good docking score, only two ligands 71588244 (Fig 12a) and 70736676 were found in the binding pocket and able to form hydrogen bonds. Ligand 22380093 and 106020530 (Fig 12b) were found outside the binding pocket. To arrive at conclusions regarding these two ligands, MD simulations must be run over a lengthy period of time. Because 22380093 has fewer rotatable bonds, it is less flexible and may not be able to achieve the conformation necessary for interaction in the binding pocket. Only ring nitrogen atoms are available for hydrogen bond formation, which could be one of the reasons for the lack of interaction at the binding site. Ligand 142663274 could also have the same reason for not giving

expected results. Ligand 129327913 found in folded condition during simulation and it was unable to reach the binding site in the given time. On the whole, few ligand did not give expected results in MD simulation in spite of good docking scores. It may due to the fact that docking studies were done in the absence of water and other ions like Chloride and Sodium. MD simulations were done both in the solvation condition and in the presence of other ions that might change the behavior of the ligands.

Overall, after analyzing the results of MD simulations, two ligands (71588244 and 70736676) were considered the best. Fig 10a and Fig 11a give details about the interaction of the above two ligands with protein SRC kinase (PDB Id: 6L8L) in

Rashmi P, Vishak Harish

2D (2 Dimension) and Fig 10b and Fig 11b gives insight about binding interaction in 3D (2 Dimension) respectively. After the MD simulation, 70736676 was found to be H-Bonded to Thr-77 and Asp-143. As we have considered only the A chain, the residue numbers will be different, as during the docking only the A chain was taken and the residue numbers were taken automatically. And after MD the visualizer considered these residues as a different unit rather than a part. So, we can see that after docking, the ligand is bound to Thr-338 and Asp-404. When viewed in the sequence viewer in MVD it was found that both sets of residues were the same with different numbering. Similarly, 71588244 was found to be H-Bonded with Lys-35, Val-63, and Asp-143, which are Lys-295, Val-323, and Asp-404, respectively, and steric interaction with Thr-77 which is Thr-338. MD simulation is done for two ligands, 70736676 and 71588244 for 25 ns, consisting of a total of 2501 frames, generated by taking every fifth frame and video shared in the supplementary material. Water, sodium, and chloride were removed while generating the video.

On the whole it can be said that indazole and imidazopyridine analogs exhibited more interactions with the amino acid residues in the binding pocket in comparison with pyrazole analogs. The number of molecules with better binding affinity was also higher in indazole and imidazopyridine than in pyrazole analogs. Since pyrazole, indazole, and imidazopyridine were expected to bind to the hinge region, interactions were seen in most of the ligands at least with one amino acid residue in the region, which is Glu-339. Though they have shown a lower number of H-bond interactions, there are numerous steric and hydrophobic interactions, often of a weak nature. Even these weak forces of interaction were visible after MD simulations. It indicates that all these ligands exhibit many weak interactions. Maybe that is the reason, many H bonds were not observed during MD simulations. Despite that, the number of ligands showing positive results was higher. The limitation was various organ toxicities, where each ligand is predicted to exhibit one or the other. Among the ligands 129327913, and 71588244 that were considered as least toxic, only 71588244 has exhibited superior and consistent binding in the active site of 6L8L. 70736676 has shown the best binding energy in docking studies, but except hERG it has been predicted to show other toxicities whereas the other one 22380093 showed better binding energy, but in MD it has not exhibited impressive results.

4. Conclusions

The current study proved that the compounds containing pyrazole, indazole, and imidazopyridine cores could be potential SRC kinase inhibitors. Predictions indicate that these analogs may be toxic. Considering the risk-benefit ratio, most of them have not been predicted to show hERG toxicity, which is significant. Indazole core-containing ligands exhibited the least toxicity, and better binding affinity, and therefore they are considered promising SRC kinase inhibitors. This study serves as a foundation for the further evaluation of these analogs. 1-[[2-(cyclopropane carbonyl amino)phenyl] methyl]indazole-3-carboxamide (71588244) and 4-[3-[2-(1H-imidazol-5-yl) imidazole-1-yl]propyl]-3,5-dimethyl-1H-pyrazole (70736676), which were the outcomes of current research work were reported earlier for Hepatitis C anti-viral activity and Inositol hexaphosphate kinase 1, 12-S lipoxygenase inhibitory activity, respectively. For consideration under repurposing for cancer treatment, further experimental studies are needed to validate the in silico findings and evaluate the efficacy and safety of these analogs in preclinical and clinical settings. In future, these molecules will be subjected to further in-depth MD analysis for longer period of time and molecular mechanics studies for confirmation. Then the chosen ligands will be screened for SRC kinase inhibition in vitro along with anti cancer activity. If necessary, for lead optimization, toxicophores will be modified with further confirmation with in silico followed by in vitro studies. Optimized and improved drug candidates will be tested in vivo for anticancer activity.

Acknowledgments

The authors are thankful to Mallige College of Pharmacy for providing the facility to carry out the research work.

References

[1] M. K. Paul, A. K. Mukhopadhyay, Tyrosine kinase - Role and significance in cancer. International Journal of Medical Sciences, 1 (2004), 101-115.

[2] R. J. Thomson, M. Moshirfar, Y. Ronquillo, Tyrosine Kinase Inhibitors, In: StatPearls. Treasure Island (FL), 2024.

[3] C. Natoli, B. Perrucci, F. Perrotti, L. Falchi, S. Iacobelli. Tyrosine Kinase Inhibitors. Current Cancer Drug Targets, 10 (2010) 462-483.

[4] R. J. Torres, S. E. Jose, SRC Tyrosine Kinase Inhibitors: New Perspectives on Their Immune, Antiviral, and

Rashmi P, Vishak Harish

- Senotherapeutic Potential, *Frontiers in Pharmacology*, 10 (2019) 1-6.
- [5] S. S. Martellucci, L. Clementi, S. Sabetta, V. Mattei, L. Botta, A. Angelucci, SRC Family Kinases as Therapeutic Targets in Advanced Solid Tumors: What We Have Learned so Far, *Cancers (Basel)*, 12 (2020) 1448.
- [6] H. Y. Li, L. L. Carr, Predictive Biomarkers of Response to SRC Inhibitors in Lung Cancer, Getting to YES1. *American Journal of Respiratory and Critical Care Medicine*, 200 (2019) 802-804.
- [7] Pelaz SG, Taberero A, SRC: coordinating metabolism in cancer, *Oncogene*, 41 (2022) 4917–4928.
- [8] J. G. Trevino, J. M. Summy, G. E. Gallick, SRC inhibitors as potential therapeutic agents for human cancers, *Mini-Reviews in Medicinal Chemistry*, 6 (2006) 681-687.
- [9] E. M. Balzer, R. A. Whipple, K. Thompson, A. E. Boggs, J. Slovic, E. H. Cho, M. A. Matrone, T. Yoneda, S. C. Mueller, S. S. Martin, c-SRC differentially regulates the functions of micro-tentacles and invadopodia, *Oncogene*, 29 (2010) 6402–6408.
- [10] J. C. Dawson, A. Munro, K. Macleod, M. Muir, P. Timpson, R. J. Williams, M. Frame, V. G. Brunton & N. O. Carragher. Pathway profiling of a novel SRC inhibitor, AZD0424, in combination with MEK inhibitors for cancer treatment, *Molecular oncology*, 16 (2022) 1072–1090.
- [11] C. Fraser, J. C. Dawson, R. Dowling, D. R. Houston, J. T. Weiss, A. F. Munro, M. Muir, L. Harrington, S. P. Webster, M. C. Frame, V. G. Brunton, E. E. Patton, N. O. Carragher, A. Unciti-Broceta. Rapid Discovery and Structure-Activity Relationships of Pyrazolopyrimidines That Potently Suppress Breast Cancer Cell Growth via SRC Kinase Inhibition with Exceptional Selectivity over ABL Kinase, *Journal of Medicinal Chemistry*, 59 (2016) 4697–4710.
- [12] M. P. Smolinski, Y. Bu, J. Clements, I. H. Gelman, T. Hegab, D. L. Cutler, J. W. S Fang, G. Fetterly, R. Kwan, A. Barnett, J. Y. N. Lau, D. G. Hanjauer, Discovery of Novel Dual Mechanism of Action SRC Signaling and Tubulin Polymerization Inhibitors (KX2-391 and KX2-361), *Journal of Medicinal Chemistry*, 61 (2018) 4704–4719.
- [13] K. R. Brandvold, M. E. Steffy, C. C. Fox, M. B. Soellner, Development of a highly selective c-SRC kinase inhibitor, *ACS Chemical Biology*, 7 (2012) 1393-1398.
- [14] M. Guo, S. Dai, D. Wu, Y. Duan, J. Li, L. Qu, L. Jiang, Z. Chen, X. Chen, Y. Chen, Characterization of ibrutinib as a non-covalent inhibitor of SRC-family kinases, *Bioorganic & Medicinal Chemistry Letters*, 34 (2021) 127757.
- [15] A. Vultur, R. Buettner, C. Kowolik, W. Liang, D. Smith, F. Boschelli, R. Jove, SKI-606 (bosutinib), a novel SRC kinase inhibitor, suppresses migration and invasion of human breast cancer cells, *Molecular Cancer Therapeutics*, 7 (2008) 1185–1194.
- [16] R. Bitencourt, I. Zalberg, I. D. Louro, Imatinib resistance: a review of alternative inhibitors in chronic myeloid leukemia, *Revista Brasileira de Hematologia e Hemoterapia*, 33 (2011) 470-5.
- [17] S. Chakraborty, E. Ahler, J. J. Simon, L. Fang, Z. E. Potter, K. A. Sitko, J. J. Stephany, M. Guttman, D. M. Fowler, D. J. Maly, Profiling of drug resistance in SRC kinase at scale uncovers a regulatory network coupling autoinhibition and catalytic domain dynamics, *Cell Chemical Biology*, 15 (2024) 207-220.e11.
- [18] R. Thomsen and M. H. Christensen, MolDock: A New Technique for High-Accuracy Molecular Docking, *Journal of Medicinal Chemistry*, 49 (2006) 3315-3321.
- [19] BIOVIA, Dassault Systèmes, [Discovery Studio Visualizer], [v21.1.0.20298], San Diego: Dassault Systèmes, [2021].
- [20] G. Xiong, Z. Wu, J. Yi, L. Fu, Z. Yang, C. Hsieh, M. Yin, X. Zeng, C. Wu, A. Lu, X. Chen, T. Hou, D. Cao, ADMETlab 2.0: An integrated online platform for accurate and comprehensive predictions of ADMET properties, *Nucleic Acids Research*, 49 (2021) W5-W14.
- [21] GROMACS 2024.1 manual. <https://doi.org/10.5281/zenodo.10721192>. Accessed: 18.04.2024
- [22] M. J. Abraham, Murtola T, Schulz R, PállV, Smith J C, B. Hess and E. Lindahl,

Rashmi P, Vishak Harish

- GROMACS: High performance molecular simulations through multi-level parallelism from laptops to supercomputers, *SoftwareX*, 1 (2015) 19–25.
- [23] S. Páll, M. J. Abraham, C. Kutzner, B. Hess, and E. Lindahl Markidis S, Laure E, Tackling exascale software challenges in molecular dynamics simulations with GROMACS; in *Solving software challenges for exascale*. Springer International Publishing Switzerland, London, 2015.
- [24] S. Pronk, S. Páll, R. Schulz, P. Larsson, P. Bjelkmar, R. Apostolov, M. R. Shirts and J. C. Smith. GROMACS 4.5: A high-throughput and highly parallel open source molecular simulation toolkit, *Bioinformatics*, 29 (2013) 845–854.
- [25] E. F. Pettersen, T. D. Goddard, C. C. Huang, G. S. Couch, D. M. Greenblatt, E. C Meng, T. E. Ferrin, UCSF Chimera--a visualization system for exploratory research and analysis, *Journal of Computational Chemistry*, 25 (2004) 1605-12.
- [26] B. R. Brooks, C. L. I. I. Brooks, A. D. Mackerell, L. Nilsson, R. J. Petrella, B. Roux, Y. Won, G. Archontis, C. Bartels, S. Boresch, A. Caflisch, L. Caves, Q. Cui, A. R. Dinner, M. Feig, S. Fischer, J. Gao, M. Hodoscek, W. Im, K. Kuczera, T. Lazaridis, J. Ma, V. Ovchinnikov, E. Paci, R. W. Pastor, C. B. Post, J. Z. Pu, M. Schaefer, B. Tidor, R. M. Venable, H. L. Woodcock, X. Wu, W. Yang, D. M. York and M. Karplus, CHARMM: The Biomolecular simulation Program, *Journal of Computational Chemistry*, 30 (2009) 1545-1615.
- [27] B. R. Brooks, R. E. Bruccoleri, B. D. Olafson, D. J. States, S. Swaminathan and M. Karplus, CHARMM: A Program for Macromolecular Energy, Minimization, and Dynamics Calculations, *Journal of Computational Chemistry*, 4 (1983) 87-217.
- [28] A. D. MacKerell Jr, B. Brooks, C. L. I. I. Brooks, L. Nilsson, B. Roux, Y. Won and M. Karplus, Schleyer PVR (Ed). CHARMM: The Energy Function and Its Parameterization with an Overview of the Program, *The Encyclopaedia of Computational Chemistry*, First ed., John Wiley & Sons Ltd., Chichester, 1998.
- [29] A. Bondi, Van der Waals Volumes and Radii, *Journal of Physical Chemistry A*, 68 (1964) 441-451.
- [30] M. Kontoyianni, Docking and Virtual Screening in Drug Discovery, *Methods in Molecular Biology*, 1647 (2017) 255-266.
- [31] M. Guo, S. Dai, D. Wu, Y. Duan, Li J, L. Qu, L. Jiang, Z. Chen, X. Chen, Y. Chen, Characterization of ibrutinib as a non-covalent inhibitor of SRC-family kinases, *Bioorganic & Medicinal Chemistry Letters*, 15 (2021) 127757.
- [32] L. Xing, J. Klug-Mcleod, B. Rai, E. A. Lunney, Kinase hinge binding scaffolds and their hydrogen bond patterns, *Bioorganic & Medicinal Chemistry*, 23 (2015) 6520-7.
- [33] L. Xing, B. Rai, E. A. Lunney. Scaffold mining of kinase hinge binders in crystal structure database, *Journal of Computer Aided Molecular Design*, 28 (2014) 13-23.
- [34] R. Roskoski Jr, SRC protein-tyrosine kinase structure, mechanism, and small molecule inhibitor, *Pharmacological Research*, 94 (2015) 94:9-25.
- [35] M. Azam, M. A. Seeliger, N. S. Gray, J. Kuriyan, G. Q. Daley. Activation of tyrosine kinases by mutation of the gatekeeper threonine, *Nature Structural & Molecular Biology*, 15 (2008) 1109-18.
- [36] D. Basak, S. Arrighi, Y. Darwiche, S. Deb. Comparison of Anticancer Drug Toxicities: Paradigm Shift in Adverse Effect Profile, *Life*, 2 (2022) 48.
- [37] A. Remesh, Toxicities of anticancer drugs and their management, *International Journal of Basic & Clinical Pharmacology*, 1 (2017) 2–12.